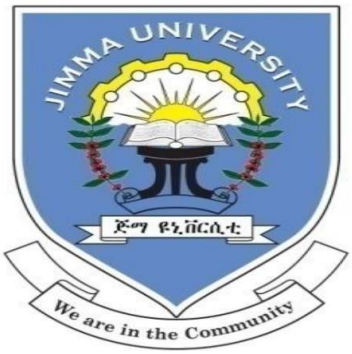

Jimma University

School of Graduate Studies

Jimma Institute of Technology

School of Biomedical Engineering

Classification of Diabetic Retinopathy and Segmentation of Hard Exudates from Retinal Fundus Images

By: Selamawit Hadush

A Thesis report submitted to the School of Graduate Studies of Jimma University in Partial Fulfillment of the Requirements for the Degree of Master of Science in Biomedical Engineering (Biomedical Imaging)

May 2020 G.C.

Jimma, Ethiopia

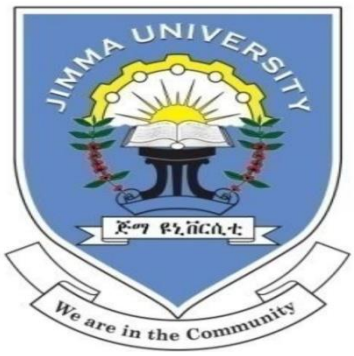

Jimma University

School of Graduate Studies

Jimma Institute of Technology

School of Biomedical Engineering

Classification of Diabetic Retinopathy and Segmentation of Hard Exudates from Retinal Fundus Images

By: Selamawit Hadush

A Thesis report submitted to the School of Graduate Studies of Jimma University in Partial Fulfillment of the Requirements for the Degree of Master of Science in Biomedical Engineering (Biomedical Imaging)

Main Advisor: Dr. Timothy Kwa (PhD)

Co-Advisor: Mohammed Aliy (MSc)

May 2020 G.C.

Jimma, Ethiopia

Declaration

I declare that this thesis report entitled "**Classification of Diabetic Retinopathy and Segmentation of Hard Exudates from Retinal Fundus Images**" is my original work and all sources of materials used for the report have been duly acknowledged and referenced as defined by the University's policy on plagiarism.

Candidate:

Selamawit Hadush Signature: _____ Date_____

On behalf of the School of Biomedical Engineering at Jimma Institute of Technology, we the advisors of this research entitled **"Classification of Diabetic Retinopathy and Segmentation of Hard Exudates from Retinal Fundus Images"** and we, the evaluators, confirm that this research is approved as MSc thesis for the student.

Advisors

Name: Dr. Timothy Kwa (PhD) Signature _____ Date_____

Name: Mr. Mohammed Aliy (MSc) Signature _____ Date _____

External Examiner

Name: _____ Signature _____ Date_____

Internal Examiner

Name:_____ Signature_____ Date_____

Abstract

Diabetic Retinopathy (DR) is a disorder of the retinal vasculature. It happens in nearly all patients with long-standing diabetes mellitus and can result in blindness. Screening of DR is essential for both early detection and early treatment of the disease. The presence of exudates is one of the complications of diabetes mellitus that is considered as the major cause of vision loss among people around the world. It results from leakage of fluid rich in fat and cholesterol from damaged retinal vasculature. The current trend for hard exudates (HE) detection is a visual grading method that is time-consuming and susceptible to observer errors. The computer-aided detection of HE would potentially assist in achieving a fast and accurate diagnosis. Even though numerous researches are done previously to come up with a method to detect DR, further improvement is needed for butter accuracy.

This thesis study develops an automatic method for DR detection and subsequently develops an effective system for the segmentation of exudates. The segmented exudates indicate the presence of DR. Before the detection of exudates, the color retinal images which were collected from international databases IDRiD, Kaggle *and e-optha Ex datasets and local images from JUMC were classified as images with DR or healthy using local binary pattern (LBP) texture descriptor and gray level co-occurrence matrix (GLCM) followed by segmentation of exudates using the morphological top-hat. Different performance metrics were used to measure the performance of the developed system. The system offered an accuracy of 98.8% for the classification of DR positive and healthy images. It offered an accuracy of 97.8%, sensitivity of 96.3%, specificity of 90%, dice score 70%, and jaccard similarity 90.9% for segmentation of exudates. The developed system also counts the number of exudates by counting white pixels in the image in each stage of the DR to just indicate how the number of exudates increases with the stage. The method was better in accuracy compared to other methods reported in the literature.*

Keywords: Diabetic retinopathy, exudates, morphological top hat

Acknowledgment

Above all, I praise God for giving me his helping hands in all of my moves from the beginning up to the end, for his guidance and grace upon me and for giving me the strength to reach this point in life during all my works and his provision to complete this work.

I extend my gratitude and appreciation to my advisors Dr. Timothy Kwa (PhD) and Mr. Mohammed Aliy (MSc) for their continual support and guidance along with the development of this thesis work. I am grateful for their professional discussions and suggestions that helped me to develop a scientific understanding of the subject.

My gratitude also goes to the Jimma University, School of Graduate Studies, Jimma Institute of Technology, School of Biomedical Engineering and Chair of Biomedical Imaging Dr. Gizeaddis Lamesgin (PhD).

Thanks to all who have been helping me in JUMC especially, Dr. Sisay and Dr. Tarekegn who were medical collaborators and supporting me while collecting local data.

My special and great thanks go to my parents for their love, support, and encouragement during my academic careers.

Finally, sincere thanks to all my friends and colleagues for sharing me constructive ideas, their inspirations, and comments on my thesis work.

Table of Content

Contents

List of Table

List of Figures

Acronyms

DME	Diabetic Macular Edema
DR	Diabetic Retinopathy
ETDRS	Early Treatment Diabetic Retinopathy Study
FCM	Fuzzy c-means
FDA	Food & Drug Administration
FOV	Field of View
GLCM	Gray Level Co-occurrence Matrix
GVF	Gradient Vector Flow
HE	Hard Exudates
HA	Hemorrhage
HOS	Higher-Order Spectra
IrMA	Intraretinal Microvascular Abnormalitie
IDM	International Diabetes Federation
JUMC	Jimma University Medical Center
LBP	Local Binary Pattern
MAs	Microaneurysms
ME	Macular Edema
NEI	National Eye Institution
NPDR	Non-Proliferative Diabetic Retinopathy
OD	Optic Disk
OCT	Optical Coherence Tomography
PNA	Preferred Network Access
PDR	Proliferative Diabetic Retinopathy
SVM	Support Vector Machine
T1DM	Type 1 Diabetes
T2DM	Type 2 Diabetes
VEGF	Vascular Endothelial Growth Factor

CHAPTER ONE

1.Introduction

1.1. Background of the Study

Diabetic retinopathy (DR) is one of the complications caused by diabetes mellitus (DM), which causes problems like stroke, cardiovascular disease, diabetic nephropathy, and diabetic neuropathy. The high glucose sugar levels due to DM damages the tiny blood vessels of the retinal capillaries and it can be visualized only in the retina, transparent tissue of several different layers of cells [1].

DM is a global epidemic with a high rate of morbidity. Since 2016, an estimated 1.6 million deaths were caused by diabetes. WHO estimates that diabetes was the seventh leading cause of death in 2016 [2]. DR is the specific microvascular complication of DM and affects 1 in 3 persons with DM. DR is one of the leading causes of vision loss in an adult population all over the world. Patients with severe levels of DR are reported to have a poorer quality of life and reduced levels of physical, emotional, and social well-being, and they utilize more health care resources [3].

DM is among the public health concerns and is leading to an increasing number of severe and chronic complications, including those that are sight-threatening. DR is among the complications of diabetes caused by high blood glucose and is a microvascular complication of both insulin-dependent (type 1) and non-insulin dependent (type 2) diabetes. It is one of the DM complications that damage blood vessels inside the retina. The retina is located at the back of the eye near the optic nerve. DR commonly affects both eyes and can lead to vision loss if it is not promptly treated. The prevalence of the disease is expected to grow exponentially, and the global population of DR patients is expected to increase to 191.0 million by 2030. The severity of DR is categorized according to the number of microaneurysms (MAs), hemorrhages, exudates, and neovascularization. The progress of DR is normally classified into the normal retina, background DR, non-proliferative DR (NPDR), proliferative DR (PDR), and macular edema (ME). Regular screening to detect retinopathy can potentially reduce the risk of the blindness of patients [4].

It is known that the occurrence of hard exudates (HE) is one of the main threats to vision loss especially when they occur near or on fovea [3]. Figure 1.1 shows an example of a color retinal fundus image with HE. HE appears at the late background and NPDR stages on the surface of the retina as bright yellowish or white at different locations [4] and with variable shapes and sizes ranging from a few pixels to thousands of pixels in the retinal images. It is well accepted that the detection of HE in color retinal images plays a vital role in DR diagnosis and monitoring the progress of treatment. HE segmentation is, therefore, the main emphasis of the current thesis study.

Since diagnostic procedures require the attention of an ophthalmologist, as well as regular monitoring of the disease, the workload and shortage of personnel will eventually exceed the current screening capabilities. To cope with these challenges, digital imaging of the eye fundus, and automatic or semi-automatic image analysis algorithms based on image processing and computer vision techniques provide great potential. By automating the analysis process, patients can be screened and referred for further examinations, and the ophthalmologists will have more time for patients that require their attention since most of the eye fundus images are not leading to any medical action [5].

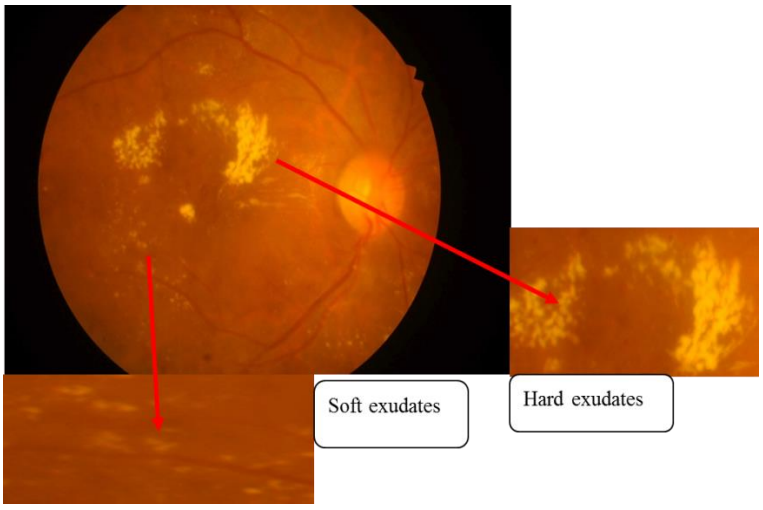

Figure 1.1: Retinal image with exudates taken at JUMC.

1.2. Structure and Function of the Eye

In the optical sciences, the human eye is often compared to a camera [6]. Light reflected from an object is focused on the retina after passing through the cornea, pupil, and lens, which is similar to light passing through the camera optics to the film or a sensor. In the retina, the incoming information is received by the photoreceptor cells which are dedicated for detecting light. From the retina, the information is further transmitted to the optic nerve, where the sensation of sight is produced. During the transmission, the information is processed in the retinal layers. A cross-section of the eye and the structures involved in the image formation are shown in Figure 1.2 [5].

There are three important features in the camera which can be seen analogous to the function of the eye: aperture, camera lens, and the camera sensor. In the eye behind the transparent cornea, the colored iris regulates the amount of light entering the eye by changing the size of the pupil. In the dark, the pupil is large allowing the maximum amount of light to enter, and when bright, the pupil is small preventing the eye to receive an excess amount of light. In the same way, the camera regulates the amount of light entering the camera with the aperture. For the eye to focus on objects at different distances, the ciliary muscle reshapes the elastic lens through the zonular fibres. For objects in short distances, the ciliary muscle contracts, zonular fibres loosen, and the lens thickens into orb-shaped which results in high refractive power. When the ciliary muscle is relaxed, the zonular fibers stretch the lens into thin shaped to see distant objects.

DR is a microvascular complication of diabetes, causing abnormalities in the retina. Typically there are no salient symptoms in the early stages, but the number and severity predominantly increase in time [6].

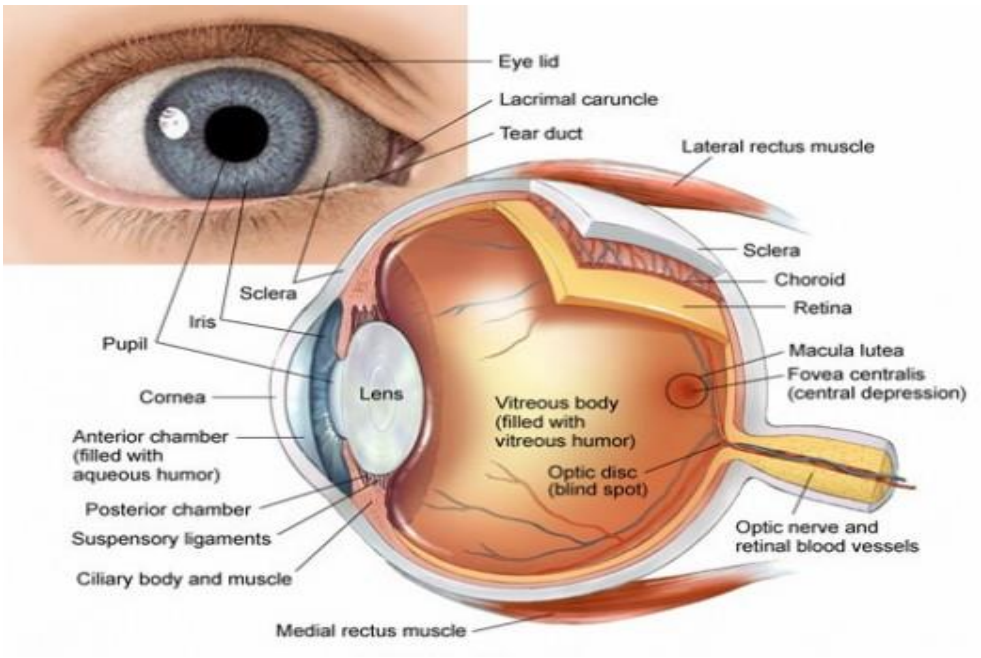

Figure 1.2: Cross-section of the eye [7].

1.3. The Eye and Diabetic Retinopathy

DR starts as small changes in the retinal capillaries. The smallest detectable abnormalities, MA, appear as small red dots in the retina and are local distensions of the weakened retinal capillary as shown in Figure 1.3 (a). Due to these damaged capillary walls, the small blood vessels may rupture and cause intra-retinal HA. In the retina, the haemorrhages appear either as small red dots indistinguishable from microaneurysms or larger round-shaped blots with irregular outline as shown in Figure 1.3 (b). The DR also increases the permeability of the capillary walls which results in retinal edema and HE. The HEs are lipid formations leaking from the weakened blood vessels and appear yellowish with well-defined borders as shown in Figure 1.3 (c). If the local capillary circulation and oxygen support fail due to obstructed blood vessels, pale areas with indistinct margins appear in the retina. These areas are small microinfarcts known as soft exudates (SE) as shown in Figure 1.3 (d). Intraretinal microvascular abnormalities (IRMA) and venopathy are signs of a more severe stage of DR, where IRMA appears as dilation in the capillary system and venopathy as shape changes in the artery and veins. The lack of oxygen and obstructed capillary in the retina lead to the development of new fragile vessels.

These new vessels attempt to grow towards the suffering tissue to supply nutrition and oxygen. However, the new vessels are fragile and tend to grow into the space between the retina and vitreous humour, or directly to the vitreous humour, which can lead to pre retinal haemorrhage and a sudden loss of vision. The growth of these new vessels is called neovascularization as shown in Figure 1.3 (e) [5].

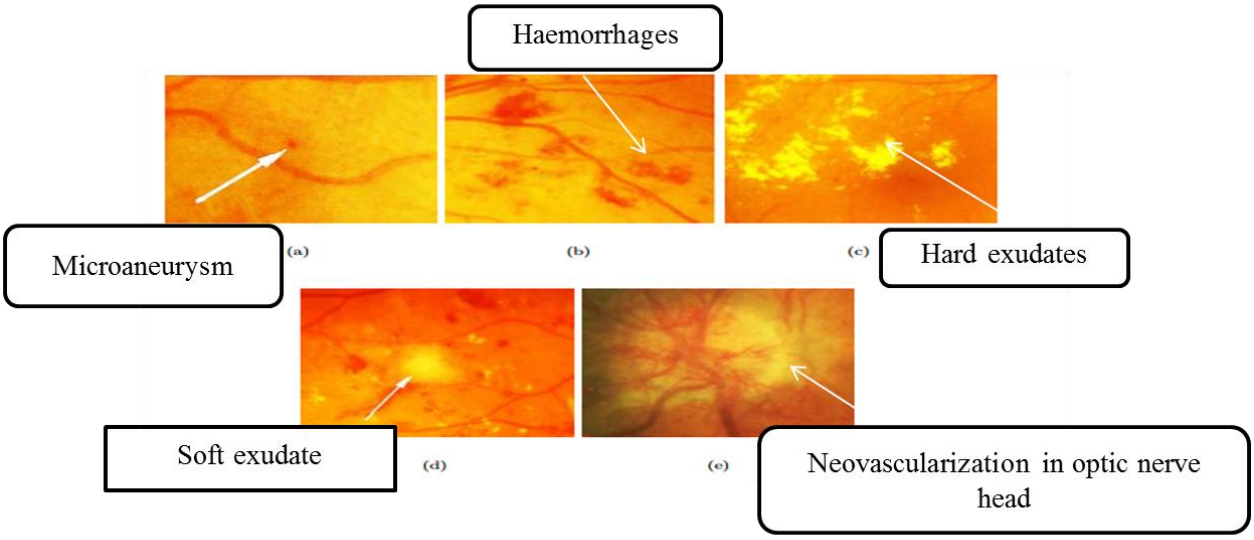

Figure 1.3: Symptoms of diabetic retinopathy (images processed for better visualization) [5].

1.4. Diabetic Retinopathy

Chronically high blood sugar from diabetes is associated with damage to the tiny blood vessels in the retina, leading to DR. The retina detects light and converts it to signals sent through the optic nerve to the brain. DR can cause blood vessels in the retina to leak fluid or hemorrhage (bleed), distorting vision. In its most advanced stage, new abnormal blood vessels proliferate (increase in number) on the surface of the retina, which can lead to scarring and cell loss in the retina. DR may progress through four stages:

Mild Non-proliferative Retinopathy: Small areas of balloon-like swelling in the retina's tiny blood vessels, called MA, occur at this earliest stage of the disease. These MAs may leak fluid into the retina.

Moderate Non-proliferative Retinopathy: As the disease progresses, blood vessels that nourish the retina may swell and distort. They may also lose their ability to transport blood. Both conditions cause characteristic changes to the appearance of the retina and may contribute to diabetic macular edema (DME).

Severe Non-proliferative Retinopathy: Many more blood vessels are blocked, depriving blood supply to areas of the retina. These areas secrete growth factors that signal the retina to grow new blood vessels.

Proliferative Diabetic Retinopathy (PDR): At this advanced stage, growth factors secreted by the retina trigger the proliferation of new blood vessels, which grow along the inside surface of the retina and into the vitreous gel, the fluid that fills the eye. The new blood vessels are fragile, which makes them more likely to leak and bleed. Accompanying scar tissue can contract and cause retinal detachment—the pulling away of the retina from underlying tissue, like wallpaper peeling away from a wall. Retinal detachment can lead to permanent vision loss. Figure 1.4 shows retinal fundus images with different stages of DR [8].

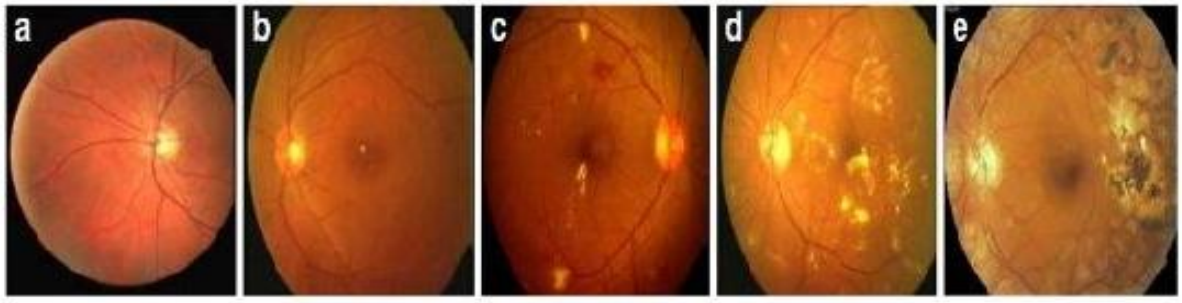

Figure 1.4: The figure shows different stages of DR (a) normal, (b) mild DR, (c) moderate DR, (d) severe DR, (e) prolific DR [9].

1.5. Diabetic Macular Edema (DME)

DME is the build-up of fluid (edema) in a region of the retina called the macula. The macula is important for the sharp, straight-ahead vision that is used for reading, recognizing faces, and driving. DME is the most common cause of vision loss among people with DR. About half of all people with DR will develop DME. Although it is more likely to occur as DR worsens, DME can happen at any stage of the disease [10].

Figure 1.5: Vision of a person with different states of diabetic retinopathy [5].

Figure 1.5 illustrates different scenarios when the same scene as viewed by a person with a normal vision (left) and with advanced DR (center). The floating spots are hemorrhages that require prompt treatment. DME (right) causes blurred vision.

1.6. DME Detection

DR and DME are detected during a comprehensive dilated eye exam that includes:

a. **Visual Acuity Testing**: This eye chart test measures a person's ability to see at various distances.
b. **Tonometry**: This test measures pressure inside the eye.
c. **Pupil Dilation**: Drops placed on the eye's surface dilate (widen) the pupil, allowing a physician to examine the retina and optic nerve.
d. **Optical Coherence Tomography (OCT):** This technique is similar to ultrasound but uses light waves instead of sound waves to capture images of tissues inside the body. OCT provides detailed images of tissues that can be penetrated by light, such as the eye. A comprehensive dilated eye exam allows the doctor to check the retina [10].

1.7. Clinical Eye Examination

The main tools in clinical eye examination are direct and indirect ophthalmoscopes and bio-microscope with indirect lenses. A direct ophthalmoscope is a handheld apparatus through which a medical expert can observe the patient's eye. The apparatus consists of the illumination source and corrective lenses, where the light beams are reflected in the patient's eye using a mirror or prism. In the indirect ophthalmoscopy, the patient's eye is examined from an arm's length by focusing high-intensity light through a hand-held condensing lens to the patient's eye and examining the reflected light (stereoscopic image) with the binocular lenses. The illumination source and the binocular lenses are mounted in a medical expert worn headband. The bio-microscope comprises an observation system and illumination system, where the observation system is a bio-microscope capable of the wide range of magnifications and the illumination system emits focal light into the patient's eye that can be controlled with slit mechanism and apertures. Combined with wide-field retinal lenses, large areas of the retina can be visualized [5].

1.7.1. Eye Fundus Photography

Eye fundus photography is considered as the preferred diagnostic modality if available since it is reliable, non-invasive and easy to use [11]. In contrast to traditional ophthalmoscopy, it allows the record of the diagnostic data and enables the expert consultation afterward, and more importantly the eye fundus photography results in a better sensitivity rate, that is, a better detection rate of abnormal eye fundus images [12]. Due to the rapid development of digital imaging, the eye fundus cameras also provide easy to file images in a portable format that enable automatic diagnosis of DR using image analysis algorithms. An eye fundus camera is illustrated in Figure 1.6. Eye fundus cameras are divided into two groups: mydriatic and non-mydriatic cameras, where the prefix denotes the requirement for dilation of the pupils with eye drops. The prefix is misleading since in practice the dilation is employed in both fundus camera types. Non-mydriatic fundus cameras are smaller and suitable for screening purposes, but at the same time the image quality is worse and the field-of-view smaller. Thus, mydriatic cameras are used when a more accurate diagnosis is needed.

The patient is seated in front of the fundus camera and the head is positioned into the instrument's headrest. A flash lamp produced light is emitted into the patient's eye using optical mirrors and lenses and the reflected light is captured by the camera sensor. The captured images are typically color images, but since the retina is transparent and the penetration depth of the emitted light depends on the wavelength, the desired retinal structures can be emphasized using optical filters. Typical alternative for color images for diagnosing DR are the red-free eye fundus images. The recommendation in the case of DR diagnosis is to use both red-free and color images [13], where two images are captured by focusing the 45^0 field-of-view fundus camera to the macula and optic disc (two-field 45^0 fundus photography) [14]. For long-term diabetic patients, two-field 60^0 photography is recommended since the neovascular changes that need treatment are typically found in the periphery, even if the changes in the central areas of the retina are slight [14].

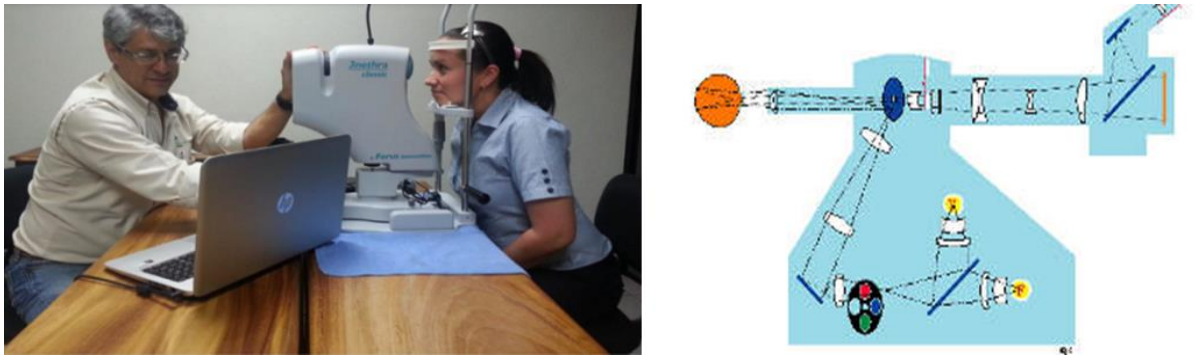

Figure 1.6: Patient examined by a fundus camera (left) and the internal structure of the fundus camera (right) [15].

1.8. DME Treatment

DME can be treated with several therapies that may be used alone or in combination. The following are the type of treatments for DR which are used currently.

1.8.1. Anti-VEGF Injection Therapy

Anti-VEGF drugs are injected into the vitreous gel to block a protein called vascular endothelial growth factor (VEGF), which can stimulate abnormal blood vessels to grow and leak fluid. Blocking VEGF can reverse abnormal blood vessel growth and decrease fluid in the retina. Available anti-VEGF drugs include Avastin (bevacizumab), Lucentis (ranibizumab), and Eylea (aflibercept). Lucentis and Eylea are approved by the US Food and Drug Administration (FDA) for treating DME. Avastin was approved by the FDA to treat cancer but is commonly used to treat eye conditions, including DME. The NEI-sponsored Diabetic Retinopathy Clinical Research Network compared Avastin, Lucentis, and Eylea in a clinical trial. The study found all three drugs to be safe and effective for treating most people with DME. Dilated eye exams may be needed less often as the disease stabilizes. Avastin, Lucentis, and Eylea vary in cost and in how often they need to be injected [16].

1.8.2. Focal/grid Macular Laser Surgery

In focal/grid macular laser surgery, a few to hundreds of small laser burns are made to leaking blood vessels in areas of edema near the center of the macula. Laser burns for DME slow the leakage of fluid, reducing swelling in the retina. The procedure is usually completed in one session, but some people may need more than one treatment. Focal/grid laser is sometimes applied before anti-VEGF injections, sometimes on the same day or a few days after an anti-VEGF injection, and sometimes only when DME fails to improve adequately after six months of anti-VEGF therapy. Table 1.1 shows how the focal laser treatment is given with different burn size, duration, and wavelength [16].

Table 1.1: Focal/grid macular laser treatment for different stages [16].

Focal Direct Laser Treatment	
Directly treat all leaking MAs in areas of retinal thickening between 500 and 3000 µm from the center of the macula (but not within 500 µm of the disc). Change in MA color with direct treatment is not required, but at least a mild gray-white burn should be evident beneath all MAs.	
Burn size	50-100 µm
Burn duration	0.05 to 0.1 sec
Wavelengths	Wavelength Green to yellow
Grid Laser Treatment	
Applied to all areas with diffuse leakage or non-perfusion area. Treat the area 500 to 3000 µm superiorly, nasally and inferiorly from the center of the macula, and 500 to 3500 µm temporally from the macular center. No burns are placed within 500 µm of the disc. Aim barely visible (light gray) laser burn and each burn should be at least two visible burn widths apart.	
Burn size	50-100 µm
Burn duration	0.05 to 0.1 sec
Wavelengths	Wavelength Green to yellow

1.8.3. Corticosteroids

Corticosteroids, either injected or implanted into the eye, may be used alone or in combination with other drugs or laser surgery to treat DME. The Ozurdex (dexamethasone) implant is for short-term use, while the Iluvien (fluocinolone acetonide) implant is longer lasting. Both are biodegradable and release a sustained dose of corticosteroids to suppress DME. Corticosteroid use in the eye increases the risk of cataract and glaucoma. DME patients who use corticosteroids should be monitored for increased pressure in the eye and glaucoma [16].

1.9. PDR Treatment

For decades, PDR has been treated with scatter laser surgery, sometimes called pan-retinal laser surgery or pan-retinal photocoagulation. Treatment involves making 1,000 to 2,000 tiny laser burns in areas of the retina away from the macula. These laser burns are intended to cause abnormal blood vessels to shrink.

Although treatment can be completed in one session, two or more sessions are sometimes required. While it can preserve central vision, scatter laser surgery may cause some loss of side (peripheral), color, and night vision. Scatter laser surgery works best before new, fragile blood vessels have started to bleed. Recent studies have shown that anti-VEGF treatment not only is effective for treating DME but is also effective for slowing progression of DR, including PDR, so anti-VEGF is increasingly used as a first-line treatment for PDR [17].

1.10. Vitrectomy

A vitrectomy is the surgical removal of the vitreous gel in the center of the eye. The procedure is used to treat severe bleeding into the vitreous and is performed under local or general anesthesia. Ports (temporary water-tight openings) are placed in the eye to allow the surgeon to insert and remove instruments, such as a tiny light or a small vacuum called a vitrector. A clear salt solution is gently pumped into the eye through one of the ports to maintain eye pressure during surgery and to replace the removed vitreous. The same instruments used during vitrectomy also may be used to remove scar tissue or to repair a detached retina [18].

1.11. Prevalence of Diabetic Retinopathy

1.11.1. Global Diabetic Retinopathy Prevalence

The global prevalence of DR and DME, for the period 2015 to 2019, was 27.0%., NPDR contributing 25.2%, PDR 1.4% and DME 4.6%. The lowest prevalence of any DR was observed in Europe at 20.6% and SEA at 12.5% and highest in Africa at 33.8%, MENA 33.8%, and the Western Pacific region at 36.2%. The predominance of NPDR was seen in all the regions examined. In 2017, 425 million adults had diabetes of whom 149 million were with DR.

As per the report, in 2045 an estimated 700 million people will be with diabetes, approximately 10% of the adult global population, of whom 245 million will have lesions of DR. DR usually affects both eyes and may cause blindness if not properly treated. DR affects up to 80% of those who had diabetes for 20 years or more. At least 90% of the cases could be reduced with proper treatment and monitoring of the eyes. The longer a person has diabetes, the higher the chances of developing DR [19].

1.11.2. Retinopathy in Ethiopia

The overall prevalence of retinopathy in 2019 was 19.48%. Based on the subgroup analysis the prevalence of retinopathy was 12.48% in SNNPR, 24.8% in Oromia, 19.99% in Amhara, and 16.29% in Addis Ababa [20]. Figure 1.7 shows trends in the age-standardized prevalence of diabetes in Ethiopia and other top five countries from Africa with high prevalence.

Top five countries for number of people with diabetes(20-79 years,2019

	Millions
South africa	4.6
Nigeria	2.7
Democratic Republic of congo	1.8
Ethiopia	1.7
United Republic of Tanzania	1.0

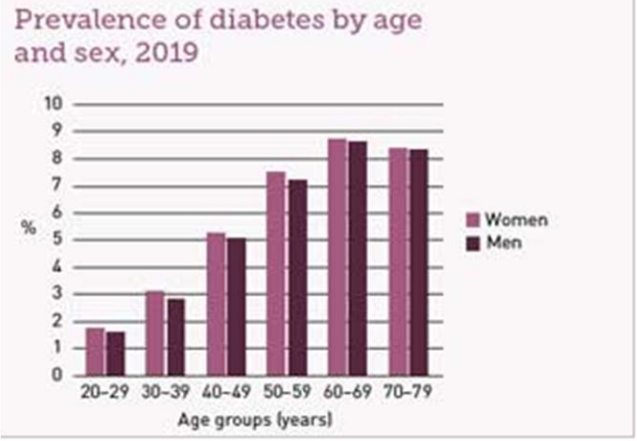

Figure 1.7: Prevelence of diabetes in top five countries including Ethiopia [21].

1.11.3. Retinopathy Cases at Jimma Medical Center

The prevalence of DR at Jimma Medical Center (JUMC) from February to March 2009 was 41.4%. Of these, 2.2% of the cases had severe non-proliferative DR while about 6% of patients had clinically significant macular edema. Vision threatening DR was found in 7.3% of patients. Only 14.5% of the patients had prior eye check. The mean duration of diabetes mellitus, mean fasting blood sugar, mean systolic blood pressure and mean diastolic blood pressure was 6.26 years, 158.8 mg/dl, 124.6 mmHg and 77.65 mmHg respectively. There was a statistically significant association between DR and duration of diabetes, fasting blood sugar, and systemic blood pressure ($p < 0.05$) [22]. According to the systematic review report, it also affects the sub-saharan diabetic patients [23].

1.12. Role of Computer-aided DR and Exudate Detection

Most early detection programs use non-mydriatic digital color fundus cameras to acquire color photographs of the back of the eye, the retina. These photographs are then examined by human experts for the presence of specific lesions that are indicative of DR. The lesions primarily include MAs, hemorrhages, exudates and cotton-wool spots, as well as blood vessel caliber changes. Other, non-DR lesions can also be detected, including nevi and melanomas.

The digital color fundus camera works well, but the weak links in the human expert reading the retinal images are difficult while evaluating hundreds up to thousands of photographs every day, intra-observer and inter-observer variability while interpreting the result, necessitating frequent and costly retraining and recertification of the human experts. Also, the delay between the patient being examined and the result of the reading can be days, thereby making it impossible to inform the patient about the test result while they are still available at the point of service [25].

Exudates are one of the parameters that deduce the presence of DR in a diabetic patient. The lipid fluids that leak from the blood vessels accumulate in the retinal region, and these deposits are known as exudates. There are two types of exudates – HE and SE. SE is the accumulation of the ruptured vessel debris. These are usually oval or round in shape and white or pearly white. These are found in fewer numbers and usually lie near the OD.

HE is small or large deposits of the lipids. These appear waxy or yellowish-white and are found in large numbers, usually underneath the blood vessels. The ophthalmologists acutely examine these exudates using a specialized camera, fundus camera. One of the most researched works conducted all around the globe is to automate the process of exudate identification, to help the patients and facilities to tackle eye-related complications [26].

1.13. Statement of the Problem

DR is a diabetes complication that affects the eyes. It's caused by damage to the blood vessels of the light-sensitive tissue at the back of the eye. If the level of insulin is less in blood vessels then diabetes occurs. At first, DR may cause no symptoms or only mild vision problems. Eventually, it can cause blindness. It is a progressive eye disease and taking proper treatment of this disease can prevent the eyes from blindness. The number of people affected by blindness due to DR increased from 0.2 million to 0.4 million, and moderate to severe vision impairment increased from 1.4 million to 2.6 million [27]. The overall prevalence of retinopathy in Ethiopia was 19.48% in 2019. Based on the subgroup analysis, the prevalence of retinopathy was 12.48% in SNNPR, 24.8% in Oromia, 19.99% in Amhara, and 16.29% in Addis Ababa [20].

Regular screening to detect retinopathy can potentially reduce the risk of blindness to patients. It is known that the occurrence of HE is one of the main threats to vision loss especially when they occur near or on the fovea. HE appears at the late background and NPDR stages on the surface of the retina as bright yellowish or white at different locations and with variable shapes and sizes ranging from a few pixels to thousands of pixels in the retinal images. It is well accepted that the detection of HE in color retinal images plays a vital role in DR diagnosis and in monitoring the progress of the DR treatment [28].

The current trend in HE detection is visual grading which is time-consuming and susceptible to observer errors [5]. The computer-aided detection of HE would potentially assist in achieving a fast and accurate diagnosis. Nowadays different techniques are used for the detection and grading of DR.

Some researchers have proposed methods for automatic detection of exudates. Such systems have a great significance on early detection of these abnormalities and could limit the severity of the disease and assist ophthalmologists in investigating and treating the disease more efficiently. Even though numerous researches are done to come up with a method to detect DR and exudates, further study is still needed for better accuracy.

1.14. Objectives

1.14.1. General Objective

The general objective of the study is to classify DR and segment HEs from retinal fundus images**.**

1.14.2. Specific Objectives

The specific objectives of the research are

- To extract features from preprocessed fundus retinal images.
- To classify the retinal fundus images.
- To segment HEs from the classified DR images.
- To evaluate the performance of the system.
- To compare the performance of the developed system with other related works.

1.15. Significance of the Study

DR is the most frequent microvascular complication of diabetes and can lead to several retinal abnormalities including MAs, exudates, dot and blot hemorrhages, and cotton wool spots. Automated detection of these abnormalities could limit the severity of the disease and assist ophthalmologists in investigating and treating the disease more efficiently. Especially detection of HEs is one of the primary signs of DR. Segmentation of HEs in retinal images can contribute to the detection of the disease. In that regard, the current thesis presents an automatic screening system for the detection of DR and HE segmentation.

1.16. Scope of the Study

This research mainly focuses on the segmentation of exudates indicating the presence of DR. Before the detection of exudates, the images will be classified as images with DR and healthy images. The study is carried out based on fundus camera generated retinal images collected from international databases and local images collected at JUMC. The retinal image processing algorithm involves image preprocessing, feature extraction using GLCM and LBP, classification of the retinal images as healthy images and images with DR using support vector machine (SVM) and segmentation of HEs using the morphological top hat. Different performance metrics were used to measure the performance of the system. To validate the performance of the system's output, the results generated from the developed system are compared to expert findings. The findings will help to detect fundus images with DR and segment the HEs using the morphological top hat operator. The method will alleviate issues with visual grading procedures which are time-consuming and susceptible to observer errors.

1.17. Organization of the Thesis

The rest of the thesis has been organized into four chapters. In Chapter 2, related works on the area of DR and exudate detection, feature extraction, and classification are reviewed. Chapter 3 explains the methodology and materials used for this research. The next chapter, Chapter 4, is about the results obtained from the study and discussions. Finally, the conclusion and feature works of the study are presented in Chapter 5.

CHAPTER TWO

2.Literature Review

A review of related works in DR pre-processing, feature extraction, classification, and segmentation of HE are discussed in this chapter. A summary is then provided that indicates the gaps in the existing methodologies. Different techniques of DR classification and exudates segmentation are discussed.

2.1. Literature Review Related to DR Classification

In the works of R. Acharya et al., four stages of DR were mentioned namely: mild non-proliferative retinopathy, moderate non-proliferative retinopathy, severe non-proliferative retinopathy and proliferative retinopathy. DR images were analyzed by using an image processing technique and support vector machine (SVM). From the raw image, four features were extracted by using the image processing technique and later feed into the SVM classifier. Using the automated system, accuracy of around 82% was achieved [29].

In a study by K. Chus et al., classification of DR has been done using Higher Order Spectra (HOS) as feature extraction and SVM as a lassifier. It has been concluded that the accuracy depends on several factors such as size, quality, and rigor of training set. It also depends on the parameters chosen to represent the input [30].

In S. Lee et al., computer classification criteria were developed for the levels of individual lesions and NPDR. Evaluation of the method was performed using 430 retinal color images of which 361 were with no retinopathy. This article described a method for a computer system using new software to grade the severity of 3 types of early lesions (HMA, HE, and CWS) of DR and a method to classify NPDR based on these 3 lesions only. Classification results from the computer system were compared with those of graders from an established fundus reading center and a general ophthalmologist. The results show that the computer system could become a useful aid for physicians and fundus image graders and a tool for large studies [31].

In the works by D. Mule et al., detection and classification of the retinal images were carried out using an advanced nonparametric method with higher classification accuracy. The objectives of the work were (i) detection of blood vessels, (ii) detection of hemorrhages, and (iii) classification of the detections into normal, moderate non-proliferative diabetic retinopathy (NPDR) and severe NPDR. Accuracy assessment of the classified outputs revealed that normal cases were classified with 90% accuracy while moderate and severe NPDR cases were 87.5% accurate [32].

2.2. Literature Related with Hard Exudates Segmentation

The interest in automatic detection of DR has been increasing along with the rapid development of digital imaging and computing. However, the single most important event that attracted the wider attention of medical, research community has been the decision to recognize digital imaging as an accepted modality to document eye fundus. Since then, a considerable amount of effort has been spent on automated detection and diagnosis of DR from digital eye fundus images. HE is usually visually graded which is time-consuming and susceptible to observer errors [33]. The computer-aided detection of HEs would potentially assist in achieving a fast and accurate diagnosis. Many published algorithms have been developed for automatic HE detection in retinal images

S. Lonf et al. developed and evaluated an automatic retinal image processing algorithm for HE detection using dynamic thresholding and fuzzy C-means clustering (FCM) followed by SVM for classification. The algorithm consisted of four main stages: imaging preprocessing, localization of the OD, determination of candidate HE using a dynamic threshold in combination with a global threshold based on FCM, and extraction of eight texture features from the candidate HE region, which were then fed into a SVM classifier for automatic HE classification. It was tested on the DIARETDB1 database (89 images) with the overall average sensitivity, specificity, and accuracy of 97.5%, 97.8%, and 97.7%, respectively. The HE detection result was poor as some big and bright cotton wool spots were wrongly detected as HE and some small HEs were ignored [28].

In A. Sopharak et al., contrast enhancement was applied to enhance the quality of the input image before four features namely, intensity, standard deviation on intensity, hue, and the number of edge pixels, were selected to supply to the FCM.

The number of required clusters was optimally selected from a quantitative experiment where it was varied from two to eight clusters. Optimization of the number of clusters was based on sensitivity and specificity which were calculated by comparison of the detected results and hand-drawn ground truths from expert ophthalmologists. The positive predictive value and positive likelihood ratio were also used to evaluate the overall performance of the method. It was found that the method detected exudates with 92.18% sensitivity and 91.52% accuracy [34].

A. Elbalaoui et al. divided their work into four steps: shifting color correction, OD elimination, exudates segmentation and separation of exudates from the background. To correct non-uniform illumination, the grey world method was used. Then extraction of OD was carried out since it appears in similar color, intensity, and contrast to exudates. Next, to segment the exudates, the mean-shift method was applied. Finally, they have used the maximum entropy thresholding to separate the exudates from the background. The proposed method was tested on DIARETDB0 and DIARETDB1 databases and an accuracy of 93.34 % was achieved [35].

W. Kusakunniran et al. used the supervised learning based on the multilayer perceptron (MLP) to identify initial seeds with high confidences to be HEs. Then, the segmentation was finalized by unsupervised learning based on the iterative graph cut (GC) using clusters of initial seeds. Also, to reduce color intra-variations of HEs in different retinal images, the color transfer (CT) method was applied to normalize the color information during the pre-processing step [36].

2.3. Summary

Though a variety of researches are available to classify DR and segment exudates, accurate and automatic segmentation of exudates is still very challenging due to the uneven intensity of the exudates. Exudates range in color from white to yellow with varying patterns, size, contrast, and shapes. Exudates are bright lesions having maximum intensity value with relatively distinct margins. There may not be visible manifestations of DR initially but its severity rises with time. Initial screening and diagnosis of DR may help to stop vision loss.

In most low resource settings, grading of DR is carried out based on visual inspection. The visual procedure is often time consuming and subjective. Most of existing algorithms for HE detection are complex and inefficient. There is still a call for the development of an automatic retinal image processing algorithm for use in HE detection and grading of DR.

CHAPTER THREE

3. The Proposed Method

This chapter describes the experimental setup, materials, and methodology used to achieve the aim of the research. It illustrates the sampling technique to choose subjects from whom the retinal fundus photography images were taken, the image capturing procedure as well as the image classification and exudates segmentation process.

3.1. Study Area

The study was conducted in Ethiopia. Local data was collected from Jimma University Medical Center (JUMC). JUMC is one of the oldest hospitals in Ethiopia and it is the only teaching and referral hospital in Southwest Ethiopia with 800-bed capacity and a catchment population of over 15 million people. Jimma city is found 350 Km away from Addis Ababa. In addition to the local data, around 412 images were downloaded from IDRID (Indian Diabetic Retinopathy Image Dataset) and e-optha ex datasets which are open for researchers and can be downloaded from an online repository [37].

3.2. Study Period

This research was conducted from March 2019 to February 2020.

3.3. Study Design

In this research, both qualitative [38] and quantitative [39] data were used. Qualitative data were collected from the different literature of related works on DR classification as well as HE segmentation. Quantitative data were also collected through observations. The observations indicated that patients do not have the habit of checkup and the sudden checkup indicates most of the DM patients were with DR. The capturing of the fundus images of DM patients at JUMC was done in collaboration with medical personnel.

3.4. Study Population

The target populations of the study were healthy people and patients with DR at different stages.

3.5. Sampling Procedure

Non-probability sampling technique [40] was used to choose a sample of subjects from a population. Using purposive sampling technique, which is non-probability sampling, the subjects are defined based on the purpose of the research. In the research, the subjects were selected purposely based on their age group and health condition. The DM patients were within the age range of 25 to 62.

3.6. DR Image Acquisition

A fundus camera provides an upright, magnified view of the eye. The observation light is focused via a series of lenses through a doughnut-shaped aperture, which then passes through a central aperture to form an annulus, before passing through the camera objective lens and the cornea on to the retina. The light reflected from the retina passes through the un-illuminated hole in the doughnut formed by the illumination system. As the light paths of the two systems are independent, there are minimal reflections of the light source captured in the formed image. The image forming rays continue towards the low powered telescopic eyepiece. When the button is pressed to take a picture, a mirror interrupts the path of the illumination system allowing the light from the flashbulb to pass into the eye. Simultaneously, a mirror falls in front of the observation telescope, which redirects the light onto the capturing medium, whether it is a film or a digital CCD. Before the fundus photography, mydriatic eye drops (such as tropicamide) are used to dilate or enlarge the pupil to obtain a better view of the fundus of the eye. Once the pupil is dilated, examiners use funduscopy to view the eye's interior, allowing assessment of the retinal details [41].

3.6.1. Experimental Design

80 subjects with DR at different stages, 37 males and 33 females, age group above 25 were considered. In addition to the DM patients', 10 healthy subjects were considered to get control images. Before 10 minutes of the examination, an eye drop is given to dilate and enlarge the pupil for further fundus examination.

3.6.2. Preparation

A fundus camera is a specialized low power microscope with an attached camera. Its optical design is based on the indirect ophthalmoscope. Fundus cameras are described by the angle of view - the optical angle of acceptance of the lens. The fundus camera used for this research was at an angle of 30°, considered the normal angle of view, creates a film image 2.5 times larger than life. Wide-angle fundus cameras capture images between 45° and 140° and provide proportionately less retinal magnification. A narrow-angle fundus camera has an angle of view of 20° or less. Figure 3.1 shows fundus images at different angle of view.

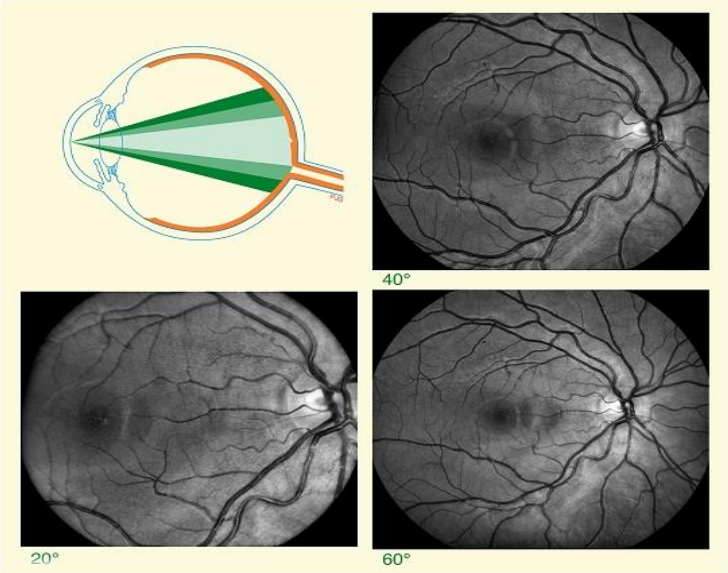

Figure 3.1: Fundus images with different angles of view [15].

Procedure:

a. Review patient records including ocular diagnosis, allergies, pregnancy status, systemic diseases;
b. Review photographic request, confirm the area of interest;
c. Plan the photographic procedure.

Prepare the patient:

a. Confirm adequate dilation;
b. Inform patient of procedures, pharmacologic agents to be administered, and potential side effects;
c. Answer patient questions concerning the procedure;
d. Position patient for photography.

3.6.3. Fundus Photography

The patient sits at the fundus camera with their chin in a chin rest and their forehead against the bar. An ophthalmic photographer focuses and aligns the fundus camera. A flash fires as the photographer presses the shutter release, creating fundus photography as shown in Figure 3.2.

Figure 3.2: Patient examined by a fundus camera at JUMC.

3.7. Ethical Considerations

A permission letter was taken for JUMC before data collection. The confidentiality of the data collected is ensured and subjects were informed about the data recording procedures and the prerequisites that they should fulfill to obtain excellent and informative data before taking the fundus images.

3.8. Overview

As the numbers of diabetes affected people are increasing worldwide, the need for automated detection methods of DR are very much significant. To have an automated system to automatically detect DR, a computer has to interpret and analyze digital images of the retina.

The developed system in this thesis consists of the following stages: preprocessing, feature extraction using gray level co-occurrence matrix (GLCM) and local binary pattern (LBP), classification of the retinal images as healthy images and images with DR and segmentation of HEs using the morphological top hat scheme. Figure 3.3 summarizes the proposed methodology on a block diagram.

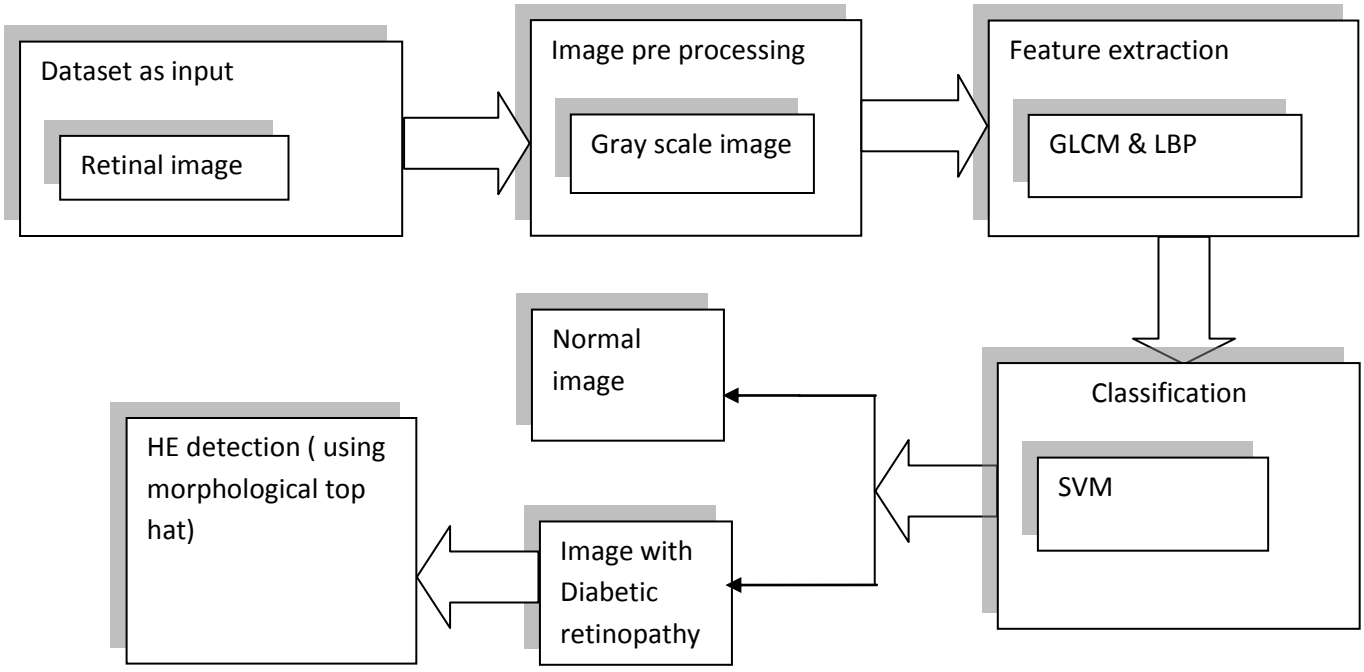

Figure 3.3: Block diagram of the methodology of the research.

3.8.1. DR Classification

3.8.1.1 Image Pre-processing

Preprocessing is used to conduct steps that reduce the complexity and increase the accuracy of the applied detection and classification algorithm. It is the process of enhancing or improving the features of image data for the next processing task. The preprocessing technique used in the DR classification system is grey-scale conversion, for reducing computation complexity. A grayscale (or gray level) image is simply one in which the only colors are shades of gray. The reason for differentiating such images from any other sort of color images is that less information needs to be provided for each pixel. `gray' color is one in which the red, green and blue components all have equal intensity in RGB space, and it is necessary to specify a single intensity value for each pixel, as opposed to the three intensities needed to specify each pixel in a full-color image [42].

3.8.2. Texture Analysis

Texture analysis and synthesis are very important for computer graphics, vision, and image processing. Texture is a measure of the variation of the intensity of a surface, quantifying properties such as smoothness, coarseness, and regularity. It's often used as a region descriptor in image analysis and computer vision. It is a repeating pattern of local variations in image intensity and cannot be defined for a point.

Texture is a property of regions; it is a contextual property and its definition must involve gray values in a spatial neighborhood. The size of this neighborhood depends upon the texture type or the size of the primitives defining the texture. It involves the spatial distribution of gray levels. Two-dimensional histograms or co-occurrence matrices are reasonable texture analysis tools.

Image texture has several perceived qualities that play an important role in describing the texture. The following properties play an important role in describing texture: uniformity, density, coarseness, roughness, regularity, linearity, directionality, direction, frequency, and phase. Some of these perceived qualities are not independent. For example, frequency is not independent of density and the property of direction only applies to directional textures.

The fact that the perception of texture has so many different dimensions is an important reason why there is no single method of texture representation which is adequate for a variety of textures. The three principal approaches used to describe texture are statistical, structural, and spectral. Statistical techniques characterize texture by the statistical properties of the grey levels of the points comprising a surface. Typically, these properties are computed from the grey level histogram or GLCM of the surface. Structural techniques characterize texture as being composed of simple primitives called "texels" (texture elements), that are regularly arranged on a surface according to some rules. Spectral techniques are based on properties of the Fourier spectrum and describe the global periodicity of the grey levels of a surface by identifying high energy peaks in the spectrum.

In many machine vision and image processing algorithms, simplifying assumptions are made about the uniformity of intensities in local image regions. However, images of real objects often do not exhibit regions of uniform intensities. For example, the image of a wooden surface is not uniform but contains variations of intensities which form certain repeated patterns called visual texture. The patterns can be the result of physical surface properties such as roughness or oriented strands which often have a tactile quality, or they could be the result of reflectance differences such as the color on a surface. GLCM of the image can represent information about direction, adjacency space, range of variation and LBP has rotational and gray invariance. Combining the LBP and GLCM statistical functions might offer a better result compared to what the individual functions could offer [43].

3.8.2.1. Local Binary Pattern

The local binary pattern (LBP) is a simple yet very efficient texture operator which labels the pixels of an image by thresholding the neighborhood of each pixel and considers the result as a binary number. Due to its discriminative power and computational simplicity, the LBP texture operator has become a popular approach in various applications. It can be seen as a unifying approach to the traditionally divergent statistical and structural models of texture analysis as it combines both. Perhaps the most important property of the LBP operator in real-world applications is its robustness to monotonic gray-scale changes caused, for example, by illumination variations. Another important property is its computational simplicity, which makes it possible to analyze images in challenging real-time settings.

The LBP was introduced as a complementary measure for local image contrast. It is invariant to monotonic changes in grayscale and it is supplemented by an independent measure of local contrast [44]. The LBP algorithm involves certain steps. Images are first labeled by thresholding the difference between a pixel and its neighbors using a step function. For the basic version, LBP neighbors mean eight direct neighbors of a pixel. Then, the values of pixels in the thresholded neighborhoods are multiplied by binomial weights given to the corresponding pixels. Finally, the values of the products are summed up to obtain the LBP number of this neighborhood.

Step 1: Thresholding

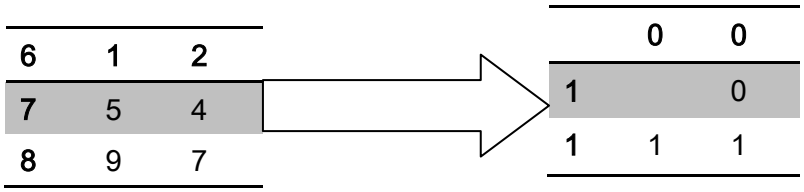

Step 2: Multiplying thresholded neighborhoods pixel value with the binomial weights

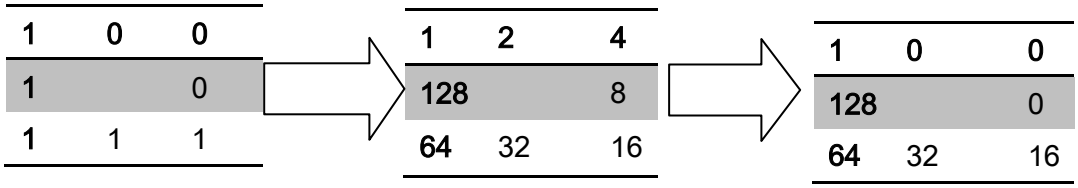

Step3: Summation of the product value gives us LBP.

LBP = 1 + 0 + 0 + 0 + 16 + 32 + 64 + 128 = 241

3.8.2.2. Gray Level Co-occurrence Matrix

The gray level co-occurrence matrix (GLCM) is a method introduced by Haralick. It is a statistical method used to measure the textural information of (grayscale) images. It considers the spatial relationship of pixels of an image by calculating how often pairs of the pixels with specific values and in a specified spatial relationship occur in an image. Statistical measures are extracted after creating a GLCM .

A co-occurrence matrix, also referred to as a co-occurrence distribution, is defined over an image to be the distribution of co-occurring values at a given offset or represents the distance and angular spatial relationship over an image sub-region of a specific size. The GLCM is created from a gray-scale image. The GLCM calculates how often a pixel with gray-level (gray-scale intensity or tone) value i occurs either horizontally, vertically, or diagonally to adjacent pixels with the value j. GLCM directions of analysis are horizontal (0^0), vertical (90^0) and diagonal: bottom left to top right (-45^0) or top left to bottom right (-135^0) which are denoted as p_0, p_{45}, p_{90} & p_{135} respectively. Figure 3.4 illustrates the directional analysis p_0, p_{45}, p_{90} & p_{135}.

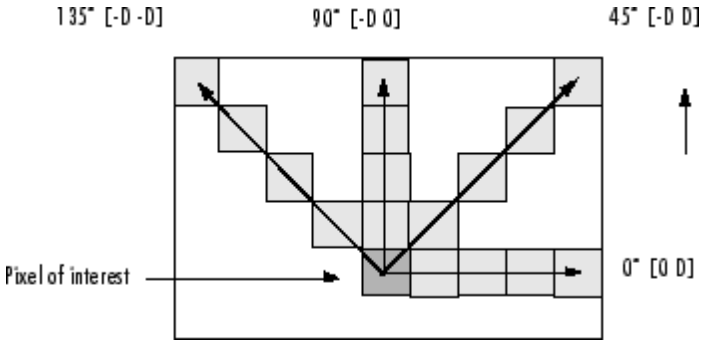

Figure 3.4: Example of directional analysis.

Steps of GLCM Calculation: The image *I* to be analyzed is a rectangular image with Mx rows and My columns. Assume that the gray levels appearing at each pixel are quantized to *Mg* levels:

Lx = {1, 2, …, Mx} is horizontal spatial domain.

Ly = {1, 2, …, My} is the vertical spatial domain.

G = {0, 1, 2, …, Mg-1} is the set of *Mg* quantized gray levels.

The set *Lx Ly* is the set of pixels of the image ordered by their row-column design. Then the image can be represented as a function of co-occurrence matrix that assigns some gray levels in *Lx Ly*. I: *Lx Ly* → G

The gray level transitions are calculated based on two parameters: displacement and angular orientation. By using a distance of one pixel and angles quantized to 45-degree intervals, four matrices of horizontal, diagonal, vertical and second diagonal are considered.

3	3	3
1	3	3
1	3	2

0^0	1	2	3
1	0	0	2
2	0	0	0
3	0	1	3

45^0	1	2	3
1	0	0	2
2	0	0	0
3	0	0	2

90^0	1	2	3
1	1	0	1
2	0	0	1
3	0	0	3

135^0	1	2	3
1	0	0	0
2	0	0	1
3	0	0	2

Figure 3.5: Gray level co-occurrence matrix: Original image (1st), 0 degree (2nd), 45 degrees (3rd), 90 degrees (4th) and 135 degrees (last).

From the GLCM, different parameters, the so called texture features or texture descriptors, can be derived. The most common once are energy, entropy, contrast, local homogeneity and correlation. Entropy measures the randomness of intensity distribution, low values for smooth images than for coarse images. Energy measures the number of repeated pairs and the uniformity of the normalized matrix. The contrast feature is a standard measurement of the number of local variations present in an image. The higher the value of contrast is, the sharper the structural variation is in the image. Local homogeneity measures the closeness of the distribution of elements in the GLCM to the GLCM diagonal. The converse of homogeneity is contrast. The correlation describes the degree of relationship between two variables [45][46].

3.8.3. Machine Learning

Machine learning studies computer algorithms for learning to do activities that humans perform naturally. Humans can learn to complete a task, to make accurate predictions or to behave intelligently. Machine learning is about learning to do better in the future based on what was experienced in the past. Learning is based on some observation, data, direct experience or instruction.

The emphasis of machine learning is on automatic methods and the goal is to devise learning algorithms that do the learning automatically without human intervention or assistance. It uses a computational method to learn information directly from data without relying on a predetermined equation as a model. The algorithms find natural patterns in data that generate insight and help to make better decisions and predictions.

Machine learning uses two types of techniques:

- Supervised learning which trains a model on known input and output data so it can predict the future output.
- Unsupervised learning which finds hidden patterns or intrinsic structures in input data.

Unsupervised Learning: Unsupervised learning finds hidden patterns or intrinsic structures in data. It is used to draw inferences from datasets consisting of input data without labeled responses.

Clustering: Clustering is the most common unsupervised learning technique. It is used for exploratory data analysis to find hidden patterns or groupings in data. Applications for clustering include gene sequence analysis, market research, and object recognition.

Supervised Learning: Supervised machine learning aims to build a model that makes predictions based on evidence in the presence of uncertainty. A supervised learning algorithm takes a known set of input data and known responses to the data (output) and trains a model to generate reasonable predictions for the response to new data. Supervised learning uses classification and regression techniques to develop.

Classification: Classification models classify input data (discrete). Typical applications include medical imaging, speech recognition, and credit scoring.

Regression: Predicts continuous responses. These include, for example, changes in temperature or fluctuations in power demand. Typical applications include electricity load forecasting and algorithmic trading.

Support Vector Machine (SVM): SVM is a supervised machine learning algorithm. It is used for classification and regression. In this method, each data item is plotted as a point in N-dimensional space where N is the number of features, the value of each feature being the value of each coordinate.

In the current thesis work, after performing image preprocessing, feature extraction was performed to obtain the features from the preprocessed images. The features include entropy, contrast, homogeneity, correlation and energy which are extracted from the GLCM and LBP is used for efficiently summarizing the local structure of images in order to classify the color fundus images using SVM. The major strength of SVM is that the training is relatively easy, with no local optimum. It also scales relatively easy to high dimensional data and the trade-off between classifier complexity and error can be controlled explicitly. Classification is performed by finding the hyperplane that differentiates two classes. There may be many possible linear classifiers that can separate two classes but the preferred one is the one that maximizes the between class distance and minimize the within class distance. This linear classifier is called the optimal separating hyperplane.

Advantages of SVM

- It's very effective in high-dimensional spaces as compared to other algorithms such as K-nearest neighbors.
- It's still effective in cases where the dimension is greater than the number of samples.
- SVM is versatile in that different kernel functions can be specified for the decision function. Common kernels are provided, but it's also possible to specify custom kernels.
- It works well with a clear margin of separation [47][48]. See also Figure 3.6.

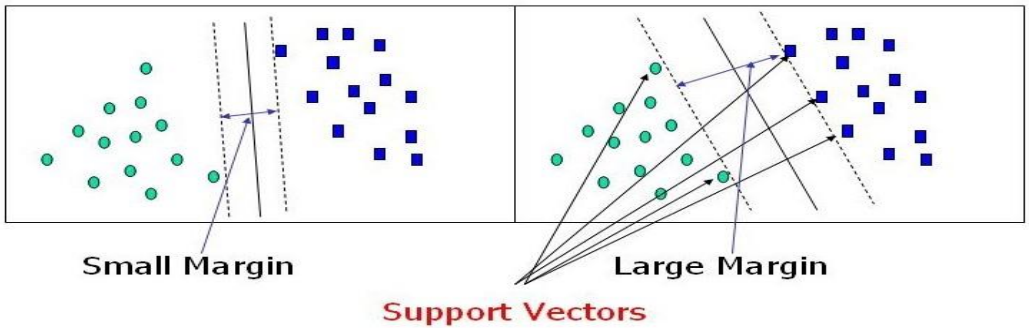

Figure 3.6. Support vectors right up against the margin of the classifier.

The key reason for using SVM in this thesis research was that the sample size of the retinal image database used is not large enough. Using SVM was expected to have better classification results because SVM can apply the nonlinear relationship between data and features better than other classifiers. Secondly, SVM can have a rapid training phase.

Exudates Detection

Retinal Image Preprocessing: The preprocessing stage used for exudate segmentation was green channel extraction. The retinal images are usually low contrast images. HE is visible in the green channel due to high contrast [49]. A sample fundus camera generated image with its red, green and blue channels is depicted in Figure 3.7 where the exudates are more visible on the green channel than the other two channels.

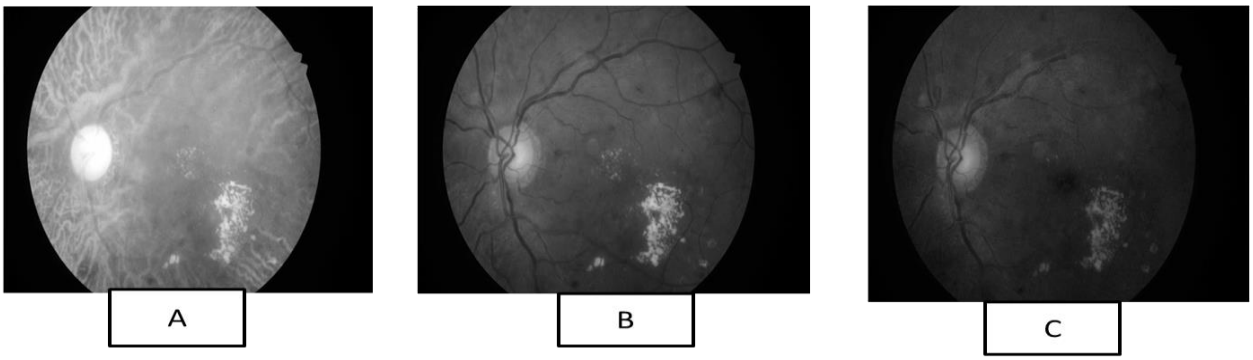

Figure 3.7: Sample fundus image with its red channel (A), green channel (B) and blue channel (C).

Mathematical Morphology: Mathematical morphology extracts components of the image which are useful for representing and describing the region's shape such as boundaries, skeletons, and convex hull. Mathematical morphology is considered as a powerful tool that solves many problems in image processing and computer vision. Erosion, dilation, closing, and top-hat transformation are the basic morphological operations that are used to detect, modify and manipulate the features presented in the image based on their shapes [13]. Mathematical morphology is a series of morphological algebraic arithmetic operators. The structuring element is applied by morphological operators typically to binary images and sometimes can be extended to gray-level images.

Selecting the proper structure element for the application, shape and size, is an important step in strengthening or weakening the results. In the case of exudates segmentation, the top-hat transformation has been applied.

Top-hat Transformation: Top-hat transform is an operation that extracts small elements and details from a given image. There exist two types of top-hat transforms: the white top-hat transform is defined as the difference between the input image and its opening by some structuring element, while the black top-hat transform is defined dually as the difference between the closing and the input image. Top-hat transforms are used for various image processing tasks, such as feature extraction, background equalization, image enhancement, and others.

Let $F: E \rightarrow R$ be a grayscale image, mapping points from a euclidean space or discrete grid E (such as R^2 or z^2) into the real line. Let $b(x)$ is a grayscale structuring element.

Then, the white top-hat transform is given by:

$$T_w(f)=f-f\ o\ b \qquad (1)$$

where o denotes the opening operation.

The black top-hat transform (sometimes called the bottom-hat transform) is given by:

$$T_b(f)=f \bullet b-f \qquad (2)$$

where ● is the closing operation.

The white top-hat transform returns an image containing those "objects" or "elements" of an input image that are "smaller" than the structuring element (i.e., places where the structuring element does not fit in), and are brighter than their surroundings. The black top-hat returns an image containing the "objects" or "elements" that are "smaller" than the structuring element, and are darker than their surroundings. The size, or width, of the elements that are extracted by the top-hat transforms can be controlled by the choice of the structuring element b. Both top-hat transformed images contain only non-negative values at all pixels. One of its most important uses in image segmentation is to adjust non-uniform lighting conditions on an image and provide a better threshold value for separating objects [50].

3.8.4. Performance Metrics

To evaluate the performance of the automatic classification of DR and exudates segmentation algorithms, several statistical measures of performance were used. The objective evaluation of the efficiency of the methodology's classification rate is analyzed using the ground truth. The metrics used were classification accuracy, sensitivity, specificity, dice score and Jaccard similarity. Before describing these metrics, here are useful terms to describe them and these results are presented in the form of confusion matrix in Chapter 5.

- True Positive (TP) detection is when the algorithm correctly detects a frame of DR.
- True Negative (TN) detection is when the algorithm correctly detects a frame of healthy images.
- False Positive (FP) detection is when a frame without DR is labeled as a frame with DR by the detection algorithm.
- False Negative (FN) detection is when a frame with DR is labeled as a frame without DR by the detection algorithm.

Classification Accuracy: is the percentage of correctly classified samples to the total sample [51].

$$Accuracy = \frac{TP+TN}{P+N} \quad (3)$$

where *P* is the total number of frames of DR and *N* denotes the total number of frames of healthy images in the test dataset.

Sensitivity: is one parameter to evaluate the rate of true positive predictions [51].

$$Sensitivity = \frac{TP}{TP+FN} \quad (4)$$

Specificity: is the rate of true negative predictions [51].

$$\boldsymbol{Specificity = \frac{TN}{TN+FP}} \quad (5)$$

Dice Score (DSC): is often used to quantify the performance of image segmentation methods by annotating some ground truth region in the segmented image.

Dice score is a measure of how similar the objects are. It is the size of the overlap of the two segmentations divided by the total size of the two objects [52].

$$DSC = \left(\frac{2TP}{2TP+FP+FN}\right) \qquad (6)$$

The dice score is not only measure of how many positives but it also penalizes for the false positives that the method finds, similar to precision. So it is more similar to precision than accuracy. The only difference is the denominator, where you have the total number of positives instead of only the positives that the method finds (see also Figure 3.8).

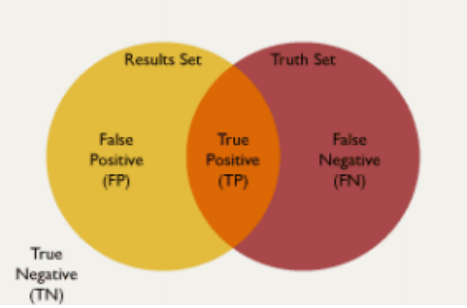

Figure 3.8: Dice score measure [52].

Jaccard Similarity Measure: Jaccard similarity coefficient measures the degree of similarity between the segmentation and the ground truth. The value is between 0 and 1 and 0 shows that segmented image and ground truth are dissimilar and 1 shows that those are identical with each other. The values between 0 and 1 show the probability of similarity between the segmented image and ground truth [52].

$$JSC = \left(\frac{TP}{TP+FP+FN}\right) \qquad (7)$$

CHAPTER FOUR

4. Result and Discussion

The proposed method has been tested on the datasets considered in this thesis. The proposed algorithm has been implemented in a Matlab 2018a environment, Toshiba Laptop (Intel Core i7 with a speed of 1.60 GHz, 2.30 GHz, 6GB RAM, and window 7 operating system).

4.1. Image Acquisition, Preparation, and Pre-processing

More than 80 real images of DR patients were captured by fundus camera connected to a computer at JUMC. To capture the image, a Kowa VX-10 alpha digital fundus camera with a 30-degree field of view (FOV) was used. All generated images have a resolution of 4288×2848 pixels and are stored in .jpg file format. A total of 7000 images were acquired from Kaggle online dataset, IDRiD dataset, and e-optha Ex dataset for training and testing purposes. Out of which 4900 images were used for training and 2100 for testing. All images came with their ground truth information. Table 4.1 shows the number and classes of images and their source.

Table 4.1: Total number of images in different classes/groups and their sources.

Presence of DR	# of images from Kaggle, IDRiD and e-optha Ex dataset	# of images from JUMC	Total # of images
Images with DR	5300	70	5370
Healthy images	1700	10	1710

Data at JUMC came from 80 patients with different duration of diabetes ranging from five years up to twenty years. Most of the patients did not have the habit of checkup for DR. It is known that having diabetes for long period of time can lead to serious health complications that include heart diseases and stroke, kidney problems, nerve damages, problems with eyesight, sores, skin infections on the feet, and gum diseases that can lead to loss of teeth. The fundus examination carried out at JUMC indicated that 87% of the diabetic patients were at different stages of DR. Figure 4.1 shows the results along with a patient examined for DR at JUMC.

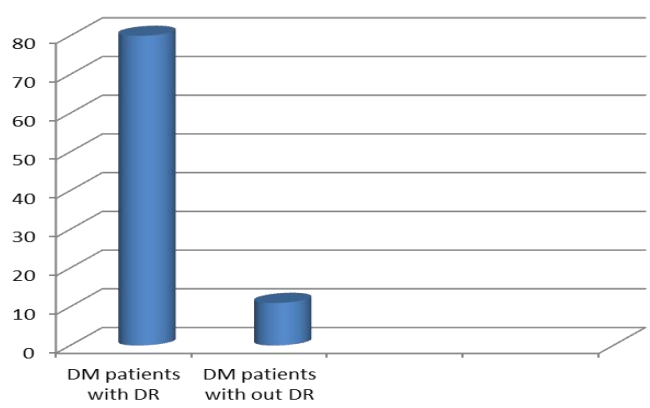

Figure 4.1.Graphical representation of the results of fundus examination at JUMC.

4.2. Feature Extraction and Classification to Detect DR

Feature Extraction using GLCM, LBP and GLCM+LBP: The performance of the computed texture descriptors is thoroughly studied in isolation and by combining of different texture descriptors. The Matlab code used to perform this feature classification is attached in the appendix (Appendix A1:A4). Table 4.2 shows the confusion matrix for the feature extraction for the classification of DR.

Table 4.2: The confusion matrix for every single method using SVM.

	DR	Healthy
DR	1269	131
Healthy	101	599

GLCM

	DR	Healthy
DR	1229	171
Healthy	136	564

LBP

	DR	Healthy
DR	1380	20
Healthy	5	695

GLCM + LBP

4.2.1. Classification Performance

The classification performance of the texture descriptors was computed for the 4900 DR and 2100 healthy images considered for training and testing purposes. Table 4.3 and performance comparison chart presented in

Figure ***4.2*** show the performance of the texture descriptors.

Table 4.3: Classification performance of different texture descriptors using SVM as a classifier.

Texture Descriptor	**Classifier**	**Classification Rate**
GLCM	SVM	Sensitivity = 92.6% Specificity = 82.05% Accuracy = 88.9%
LBP	SVM	Sensitivity = 90.04% Specificity = 76.73% Accuracy = 85.38%
LBP + GLCM	SVM	Sensitivity = 99.6 Specificity = 97.2% Accuracy = 98.8%

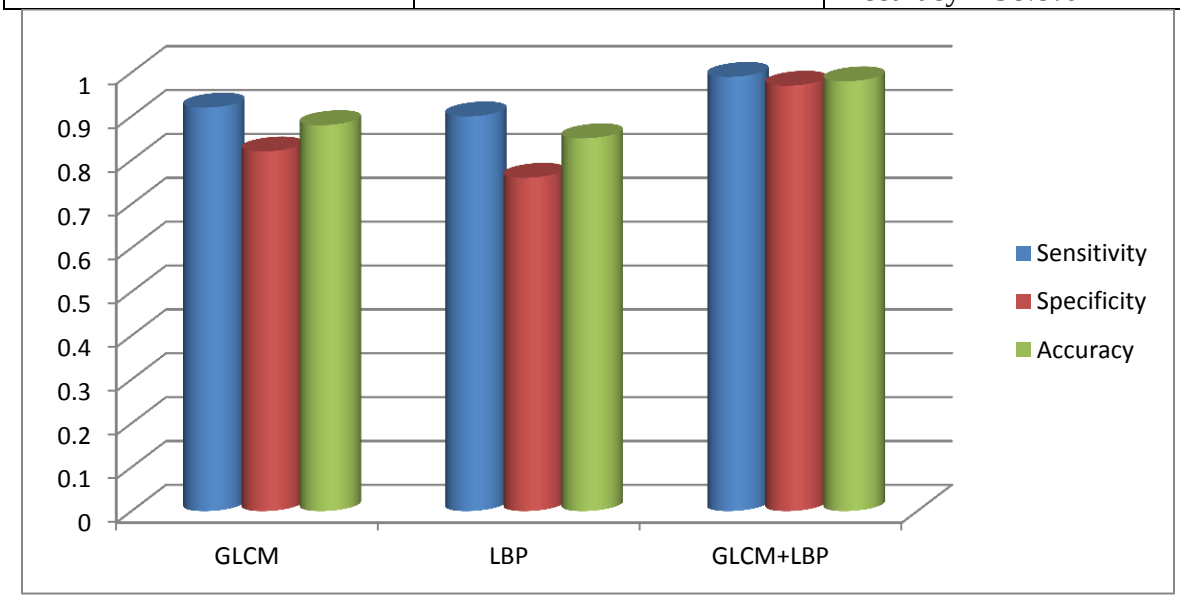

Figure 4.2: Performance comparison chart of the extracted features using SVM as a classifier.

4.3. Exudate Segmentation

The performance analysis was done on a set of 120 retinal fundus images with HE from IDRiD and e-optha Ex online datasets. The performance of the method was evaluated quantitatively by measuring accuracy, sensitivity, and specificity at the pixel level and dice score and Jaccard similarity.

This pixel-based evaluation considers four values: True positive (TP) – number of exudates pixels correctly detected; False positive (FP) – number of non-exudate pixels which are detected wrongly as exudates pixels; False negative (FN) – number of exudate pixels that are not detected as exudates; 4) True negative (TN) – number of non-exudate pixels that are correctly identified as non-exudates pixels.

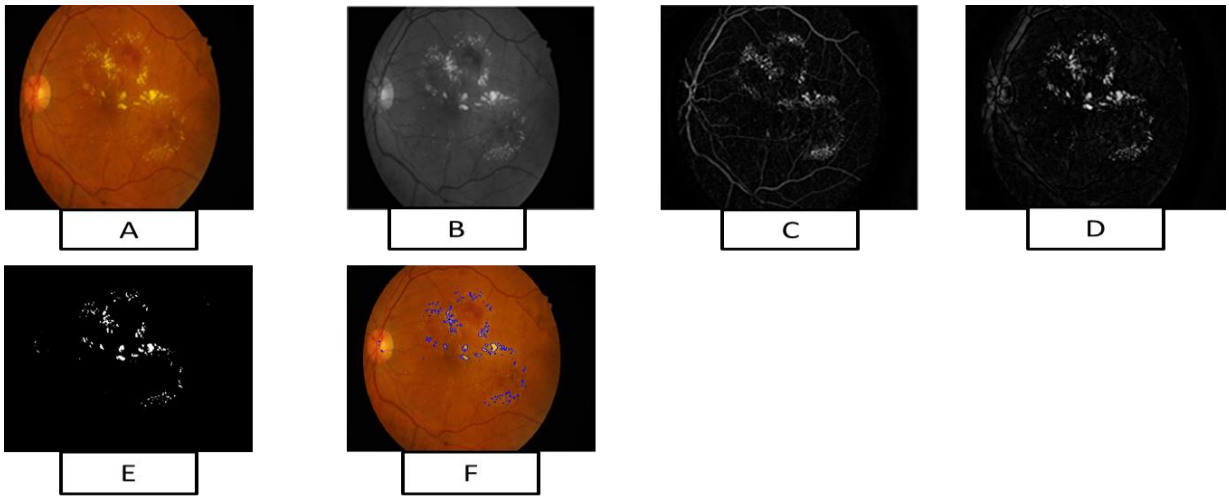

Figure 4.3: The exudate segmentation process: (A) Input image, (B) Green channel, (C) Fundus region after applying morphological bottom hat, (D) Fundus region after applying morphological top hat, (E) The segmented exudate, (F) the segmented exudates overlaid on the original image.

Figure 4.4: Result of exudate segmentation and the overlap with the ground truth.

As shown in Figure 4.3, the retinal fundus image passes through different stages for the exudate segmentation process: extraction of the green channel, applying morphological bottom hat and top hat. Finally, exudates were segmented. Figure 4.4 shows how much the segmented exudates overlap with the ground truth for further performance measurement of the developed algorithm.

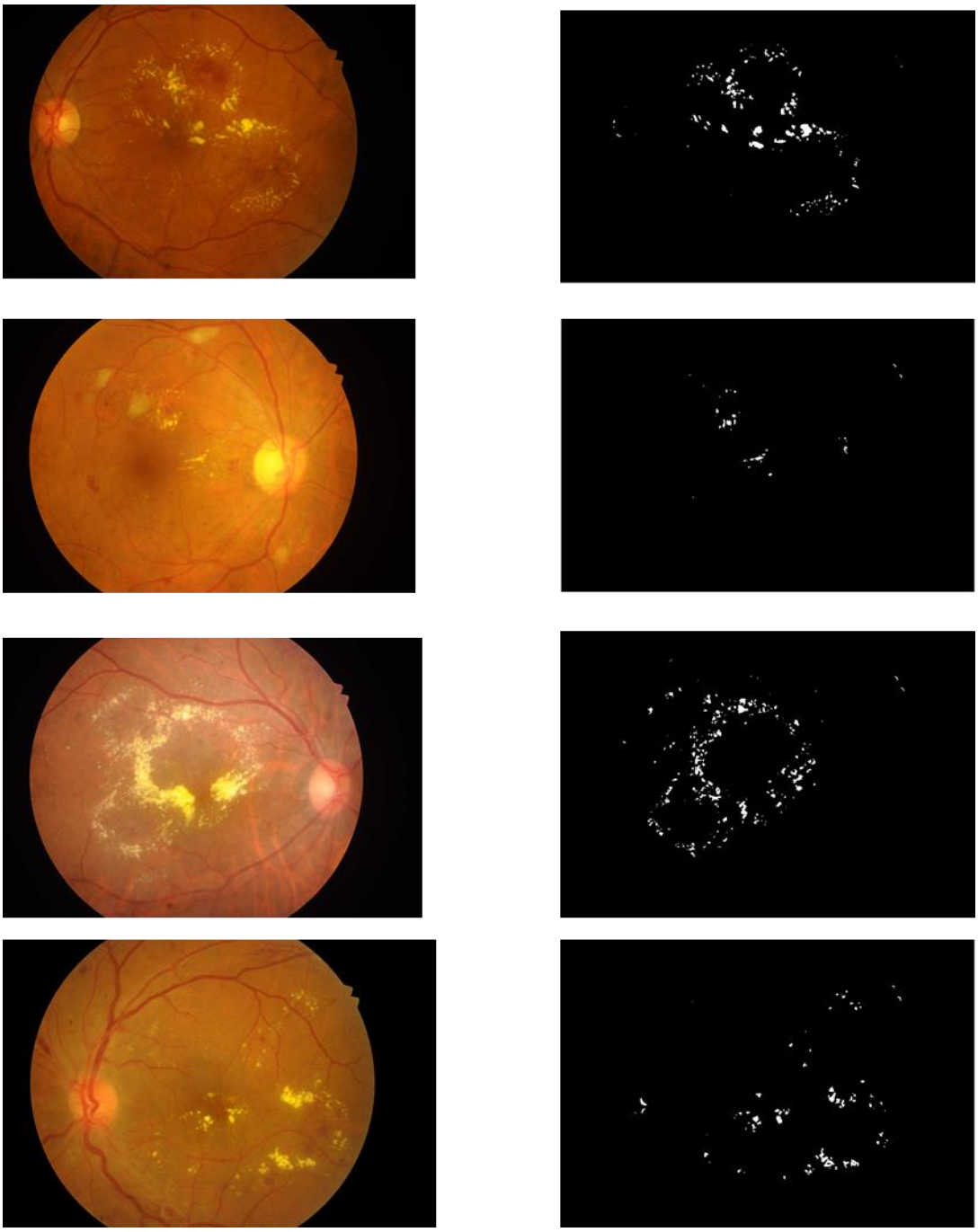

Figure 4.5: Sample retinal images and the exudates segmentation results.

As shown in Figure 4.5, the exudate segmentation result is satisfactory and the algorithm can nearly segment exudates of the retinal images fully. It achieved an accuracy of 97.8%, sensitivity of 96.3%, specificity of 90%, dice score of 70% and Jaccard similarity of 90.9% as also shown in Table 4.4.

Table 4.4: Performance measures of the developed algorithm.

# of test images	Performance Parameters				
	Sensitivity	Specificity	Accuracy	Dice score	Jaccard Similarity
120	96.3%	90%	97.8%	70%	90.9%

4.4. Segmented Exudates for Different Stages of DR

To classify the segmented images, the number of white pixels was calculated. The presence of HE shows severity of the disease as shown in Figure 4.6. As a result, experts can predict the severity of the DR based on the number of white pixels or the number of exudates. The mean value of the number of detected exudate pixels for each of the five categories of the retinal images were calculated as shown in Figure 4.7.

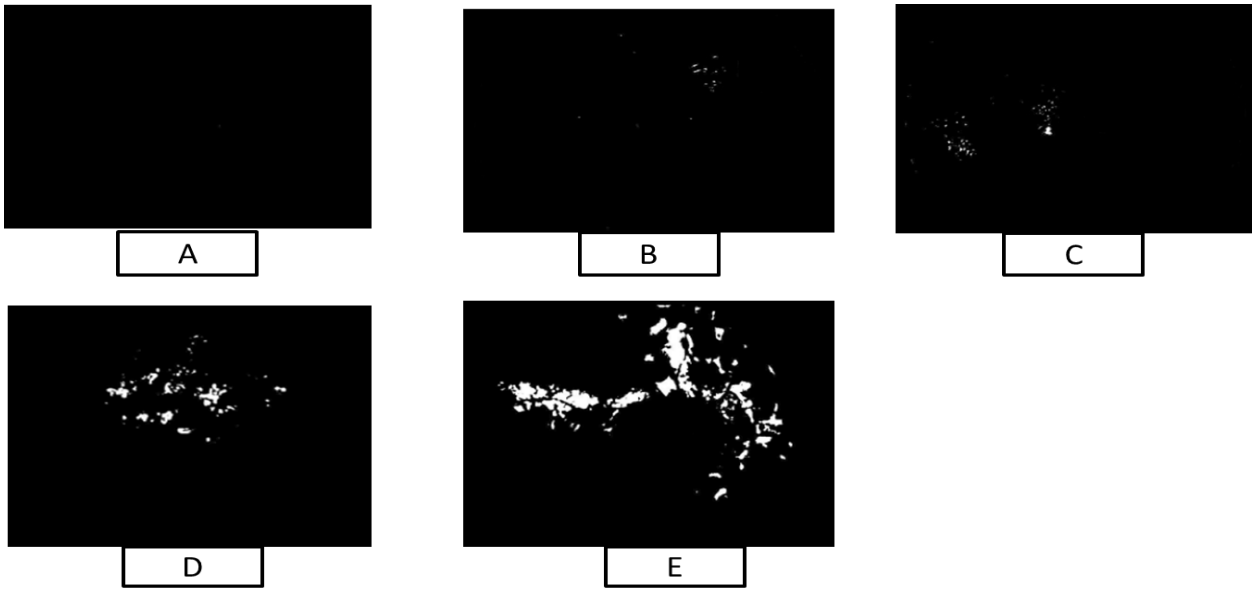

Figure 4.6: Binarized retinal images with extracted exudates: (A) normal; (B) mild; (C) moderate; (D) severe;(E) very severe

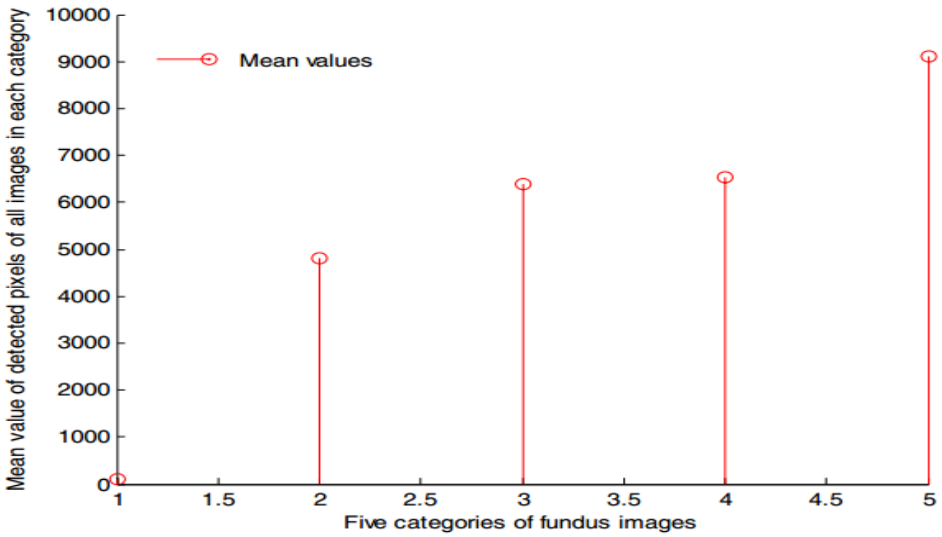

Figure 4.7: Mean value of the number of detected exudates pixels for different stages of DR.

Comparative Analysis

Table 4.5 presents a comparison between the proposed method against other methods previously proposed in the literature. In terms of overall accuracy, the proposed method offered better performance compared to all other methods. Specificity of the method was inferior to the other methods while the sensitivity was commendable enough.

Table 4.5: Comparative analysis with other methods.

Author	**Method**	**Classifier**	**SN (%)**	**SP (%)**	**ACC (%)**
Philips et al. [6]	Noise removal, thresholding	—	87	—	—
Gardner [48]	Preprocessing with edge detection filter (n=179)	NN	93.1	93.1	—
Osareh et al. (2017) [53]	FCM	SVM	92.4	90.7	95.5
Abderrahmane et al. [35]	Mean-shift method	—	94.7	97	94.4
Kusakunniran et al. (2018) [37]			89.1	99.7	96.2
Long et al.[28]	Dynamic threshold, FCM	SVM	97.5	97.8	97.7
Proposed method	Top hat transformation, Texture analysis using LBP + GLCM	SVM	96.3	90	97.8

4.5. Graphical User Interface (GUI)

A graphical user interface (GUI) is an interface through which a user interacts with the system. This interface uses icons, menus and other visual indicator representations to display information and related user controls. A GUI was developed for the proposed system. The 'load image' button enables the user to browse and load and display the saved images, and the user will continue for the pre-processing, feature extraction, classification and exudate segmentation. This system will enable users to interact with the system easily as shown in Figure 4.8.

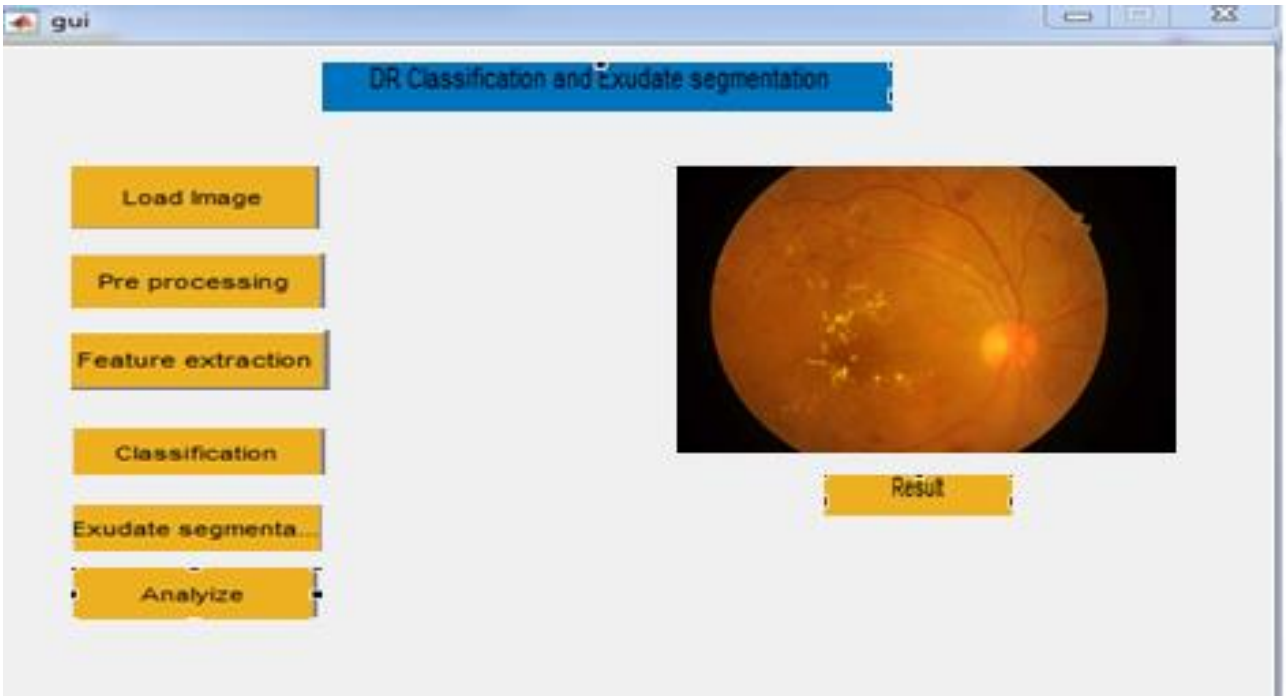

Figure 4.8: Graphical user interface of the system.

CHAPTER FIVE

5.Conclusion and Future Works

5.1. Conclusion

Diabetes is the leading cause of blindness in adults. This is a growing problem as the number of people living with diabetes increases, so does the number of people with impaired vision. Diabetes can cause a disease of the eye called DR. In its early stages, one may not notice any symptoms or changes to the eyesight and cannot know that this condition is damaging the eyes. If it is not detected and treated on time, the vision of the patient can be damaged permanently. The presence of exudates is one of the complications of diabetes mellitus that is considered as the major cause of vision loss among people around the world

HE is usually visually graded which is time-consuming and susceptible to observer errors. The computer-aided detection of HEs would potentially assist in achieving a fast and accurate diagnosis. Many algorithms have been developed in the literature for automatic HE detection in retinal images but due to the large variety of the exudates in size, intensity, shape, and contrast the segmentation process is quite challenging, leading to unsatisfactory detection accuracy for clinical applications. Also, most of the methods do not first classify the images as DR and healthy images. The proposed method is this thesis study offered an accuracy of 98.8%, specificity of 97.2%, sensitivity of 99.6% for the classification of DR and healthy images. The method also offered an accuracy of 97.8%, sensitivity of 96.3%, specificity of 90%, dice score of 70 and Jaccard similarity of 90.9% for segmentation of exudates. The methodology is suitable for HE detection as an intermediate step with relatively high accuracy compared to other algorithms developed in the literature. The system can help physicians in the diagnosis and detection of DR and in designing a treatment plan for patients.

5.2. Future Work

This thesis aimed to classify fundus images as DR and healthy images, segment the exudates and SVM was used for classification purposes. It is hoped that the system can assist ophthalmologists to automatically detect signs of DR in their early stages, in disease monitoring and better treatment plan. However, there are still rooms to improve the performance, particularly the specificity, of the method. Checking the efficacy of different classifiers after extracting more imaging features than what have been done in the current study could be one possible direction for future investigation. Diabetic maculopathy is the condition of retinopathy where exudates are present within the macular region. The severity of the maculopathy depends on how close exudates are to the center of the macula. In that regard, automatic analysis of the severity of diabetic maculopathy requires further investigation.

References

[1] "2013-SCI-301-FINAL-DR-GUIDELINES-DEC-2012-updated-July-2013.pdf," *DR Guidel.*, vol. 2012, no. July, pp. 1–147, 2012.

[2] "Diabetes." [Online]. Available: https://www.who.int/news-room/fact-sheets/detail/diabetes. [Accessed: 02-Mar-2020].

[3] R. Lee, T. Y. Wong, and C. Sabanayagam, "Epidemiology of diabetic retinopathy, diabetic macular edema and related vision loss," *Eye Vis.*, vol. 2, no. 1, Dec. 2015.

[4] S. A. Tabish, "Is Diabetes Becoming the Biggest Epidemic of the Twenty-first Century?," *Int. J. Health Sci. (Qassim).*, vol. 1, no. 2, pp. V–VIII, 2007.

[5] T. Kauppi, *Eye Fundus Image Analysis for Automatic Detection of Diabetic Retinopathy*. Lappeenranta University of Technology, Lappeenranta, Finland, 2010.

[6] N. J. Wade, "Image, eye, and retina," *J Opt Soc Am A Opt Image Sci Vis*, vol. 24, no. 5, pp. 1229–49, 2007.

[7] E. Custers, "Anatomy of the Eye: Human Eye Anatomy | Owlcation," *Owlcation*, 2017. [Online]. Available: https://owlcation.com/stem/Anatomy-of-the-Eye-Human-Eye-Anatomy. [Accessed: 02-Mar-2020].

[8] N. J. Astbury, "The Royal College of Ophthalmologists Cataract Surgery Guidelines: What can patients see with their operated eye during cataract surgery? [24]," *Eye*, vol. 17, no. 2. Royal College of Ophthalmologists, pp. 285–286, 2003.

[9] U. R. Acharya, C. M. Lim, E. Y. K. Ng, C. Chee, and T. Tamura, "Computer-based detection of diabetes retinopathy stages using digital fundus images," *Proc. Inst. Mech. Eng. Part H J. Eng. Med.*, vol. 223, no. 5, pp. 545–553, 2009.

[10] A. Das, P. G. McGuire, and S. Rangasamy, "Diabetic Macular Edema: Pathophysiology and Novel Therapeutic Targets," *Ophthalmology*, vol. 122, no. 7, pp. 1375–1394, 2015.

[11] R. Naznin and I. Parida, "An Effective Automated Technique for Retinal Disease Identification in Diabetic Retinopathy without Manually Labeled Kit," *Int. J. Comput. Appl.*, vol. 97, no. 14, pp. 1–5, 2014.

[12] A. Hutchinson *et al.*, "Effectiveness of screening and monitoring tests for diabetic retinopathy - A systematic review," *Diabetic Medicine*, vol. 17, no. 7. UK. Diabetic Medicine, pp. 495–506, 2000.

[13] G. von Wendt, P. Summanen, K. Hallnäs, P. Algvere, K. Heikkilä, and S. Seregard, "Detection of diabetic retinopathy: A comparison between red-free digital images and colour transparencies," *Graefe's Arch. Clin. Exp. Ophthalmol.*, vol. 243, no. 5, pp. 427–432, 2005.

[14] G. Wendt, *Screening for diabetic retinopathy: Aspects of photographic methods*. stockholm: Carolinska Medico Chirurgiska Institutet, 2005.

[15] P. J. S. and M. E. Tyle, "Fundus Photography Overview," *Fundus Photogr. Overv.*, vol. 18, no. 7, pp. 1–5, 2015.

[16] W. W. Drive, "DIABETIC MACULAR EDEMA (DME) DIABETIC MACULAR EDEMA (DME)," *Eye Vis.*, vol. 19, no. 7, pp. 1–3, 2015.

[17] M. H. Berrocal and L. A. Acabá, "CHAPTER 2 Proliferative Diabetic Retinopathy (PDR)," *Bentham Sci.*, vol. 1, no. 787, pp. 18–28, 2016.

[18] V. D. Karthigeyan1, "Vitrectomy Eye Surgery," *Community Eye Heal. J.*, vol. 45, no. 11, 2015.

[19] R. L. Thomas, S. Halim, S. Gurudas, S. Sivaprasad, and D. R. Owens, "IDF Diabetes Atlas : A review of studies utilising retinal photography on the global prevalence of diabetes related retinopathy between 2015 and 2018," *Diabetes Res. Clin. Pract.*, vol. 157, no. 14, p. 107840, 2019.

[20] R. O. Fite, E. A. Lake, and L. K. Hanfore, "Diabetic retinopathy in Ethiopia: A systematic review and meta-analysis," *Diabetes and Metabolic Syndrome: Clinical Research and Reviews*, vol. 13, no. 3. Elsevier, pp. 1885–1891, 01-May-2019.

[21] D. A. G. Dr. Michal S. Nowak, "Review of the epidemiology of diabetic retinopathy," *Diabetes Res. Clin. Pract.*, vol. 14, no. 4, pp. 3–5, 2020.

[22] G. Sharew, D. R. Ilako, K. Kimani, and Y. Gelaw, "Prevalence of diabetic retinopathy in Jimma University Hospital, Southwest Ethiopia.," *Ethiop. Med. J.*, vol. 51, no. 2, pp. 105–13, Apr. 2013.

[23] V. Hall, R. Thomsen, O. Henriksen, and N. Lohse, "Diabetes in Sub Saharan Africa 1999-2011: Epidemiology and public health implications. A systematic review," *BMC Public Health*, vol. 11, no. 1, p. 564, Dec. 2011.

[24] S. Abdella and M. Mohammed, “Awareness of Diabetic Patients About Their Illness and Associated Complications in Ethiopia,” *Med. Sci. | Int. Med. J.*, vol. 2, no. 2, p. 1, 2013.

[25] M. D. Abramoff, M. Niemeijer, and S. R. Russell, “Automated detection of diabetic retinopathy: Barriers to translation into clinical practice,” *Expert Rev. Med. Devices*, vol. 7, no. 2, pp. 287–296, 2010.

[26] Vasanthi Satyananda, K V Narayanaswamy, and K Karibasappa, “Extraction of Exudates from the Fundus Images A Review,” *Int. J. Eng. Res.*, vol. V5, no. 12, pp. 133–138, 2016.

[27] M. S. Nowak and A. Grzybowski, “Review of the epidemiology of diabetic retinopathy_page2.” p. 2, 2018.

[28] S. Long, X. Huang, Z. Chen, S. Pardhan, and D. Zheng, “Automatic Detection of Hard Exudates in Color Retinal Images Using Dynamic Threshold and SVM Classification: Algorithm Development and Evaluation,” *Biomed Res. Int.*, vol. 2019, pp. 1–13, Jan. 2019.

[29] E. Espinoza, G. Martinez, J. G. Frerichs, and T. Scheper, “Cell cluster segmentation based on global and local thresholding for in-situ microscopy,” *2006 3rd IEEE Int. Symp. Biomed. Imaging From Nano to Macro - Proc.*, vol. 2006, pp. 542–545, 2006.

[30] S. Report, “Digital Colour Images,” *Image (Rochester, N.Y.)*, pp. 1220–1223, 2003.

[31] S. C. Lee, E. T. Lee, Y. Wang, R. Klein, R. M. Kingsley, and A. Warn, “Computer classification of nonproliferative diabetic retinopathy,” *Arch. Ophthalmol.*, vol. 123, no. 6, pp. 759–764, 2005.

[32] D. B. Mule, S. S. Chowhan, and D. R. Somwanshi, “Detection and Classfication of Non-proliferative Diabetic Retinopathy Using Retinal Images,” *Commun. Comput. Inf. Sci.*, vol. 1036, pp. 312–320, 2019.

[33] A. Rodríguez, A. Calle, L. Vázquez, F. Chacón, P. Polavieja, and J. Reviriego, “Blood glucose control and quality of health care in non-insulin-treated patients with Type2 diabetes in Spain: A retrospective and cross-sectional observational study,” *Diabet. Med.*, vol. 28, no. 6, pp. 731–740, 2011.

[34] A. Sopharak, B. Uyyanonvara, and S. Barman, “Automatic exudate detection for diabetic retinopathy screening,” *ScienceAsia*, vol. 35, no. 1, pp. 80–88, 2009.

[35] A. Elbalaoui and M. Fakir, “Exudates detection in fundus images using mean-shift segmentation

and adaptive thresholding," *Comput. Methods Biomech. Biomed. Eng. Imaging Vis.*, vol. 7, no. 2, pp. 145–153, 2019.

[36] W. Kusakunniran, Q. Wu, P. Ritthipravat, and J. Zhang, "Hard exudates segmentation based on learned initial seeds and iterative graph cut," *Comput. Methods Programs Biomed.*, vol. 158, pp. 173–183, 2018.

[37] "IDRiD - Home." [Online]. Available: https://idrid.grand-challenge.org/. [Accessed: 20-Feb-2020].

[38] E. Hashimov, "Qualitative Data Analysis: A Methods Sourcebook and The Coding Manual for Qualitative Researchers," *Tech. Commun. Q.*, vol. 24, no. 1, pp. 109–112, 2015.

[39] K. Jones, "Book reviews : Bryman, A. and Cramer,D. 1990: Quantitative data analysis for social scientists. London: Rout ledge, xiv + 290 pp. £35.00 cloth, £10.99 paper. ISBN: 0 415 02664 4," *Prog. Hum. Geogr.*, vol. 16, no. 1, pp. 124–125, 1992.

[40] M. D. C. Tongco, "Purposive Sampling as a Tool for Informant Selection," vol. 5, pp. 147–158, 2007.

[41] K. MaheshK and K. Nilesh S, "Review on Fundus Image Acquisition Techniques with Data base Reference to Retinal Abnormalities in Diabetic Retinopathy," *Int. J. Comput. Appl.*, vol. 68, no. 8, pp. 17–27, 2013.

[42] S. H. Rasta, M. E. Partovi, H. Seyedarabi, and A. Javadzadeh, "A comparative study on preprocessing techniques in diabetic retinopathy retinal images: Illumination correction and contrast enhancement," *J. Med. Signals Sens.*, vol. 5, no. 1, pp. 40–48, 2015.

[43] M. Pietikainen, "Handbook of Pattern Recognition and Computer Vision," *Handb. Pattern Recognit. Comput. Vis.*, no. July, 2010.

[44] D. Huang, C. Shan, M. Ardabilian, Y. Wang, and L. Chen, "Local binary patterns and its application to facial image analysis: A survey," *IEEE Trans. Syst. Man Cybern. Part C Appl. Rev.*, vol. 41, no. 6, pp. 765–781, 2011.

[45] M. Held and T. I. B. Committee, "Momentum Method to Measure the Blastcontour," *17th Int. Symp. Ballist.*, vol. 2, no. March, pp. 267–274, 1998.

[46] B. Pathak and D. Barooah, "Texture analysis based on the gray-level co-occurence martix

considering possible orientations," *Int. J. Adv. Res. Electr. Electron. Instrum. Eng.*, vol. 2, no. 9, pp. 4206–4212, 2013.

[47] M. L. Series and J. Jeychandra, "Support Vector Machines," *Biomed Res. Int.*, vol. 5, no. 19, pp. 1–19, 2019.

[48] M. Faisal, D. Wahono, I. K. E. Purnama, M. Hariadi, and M. H. Purnomo, "Classification of diabetic retinopathy patients using support vector machines (SVM) based on digital retinal image," *J. Theor. Appl. Inf. Technol.*, vol. 59, no. 1, pp. 197–204, 2014.

[49] M. García, C. I. Sánchez, J. Poza, M. I. López, and R. Hornero, "Detection of hard exudates in retinal images using a radial basis function classifier," *Ann. Biomed. Eng.*, vol. 37, no. 7, pp. 1448–1463, 2009.

[50] X. Bai, "New class of top-hat transformation to enhance infrared small targets," *J. Electron. Imaging*, vol. 17, no. 3, p. 030501, 2008.

[51] A. W. Reza, C. Eswaran, and K. Dimyati, "Diagnosis of diabetic retinopathy: Automatic extraction of optic disc and exudates from retinal images using marker-controlled watershed transformation," *J. Med. Syst.*, vol. 35, no. 6, pp. 1491–1501, 2011.

[52] J. Bertels *et al.*, "Optimizing the Dice Score and Jaccard Index for Medical Image Segmentation: Theory and Practice," *Lect. Notes Comput. Sci. (including Subser. Lect. Notes Artif. Intell. Lect. Notes Bioinformatics)*, vol. 11765 LNCS, no. November, pp. 92–100, 2019.

[53] A. Osareh and B. Shadgar, "AUTOMATIC BLOOD VESSEL SEGMENTATION IN COLOR IMAGES OF RETINA," *EEE Trans. Biomed. Eng.*, vol. 33, no. 11, pp. 191–206, 2009.

Appendix

Source Code

A.1 Implementation Code for LBP using SVM

```
clear all;
clc;
close all;
data=[];
for i=1:4900
a=imread(strcat([' F:/thesis3/selam/Trainingset/'num2str(i)],'.jpg'));
I = rgb2gray(a);
K=imresize(double(I),[ 512 512]);
features = extractLBPFeatures(K);
data=[data;features];
end
X=data;
P=csvread('F:/thesis3/selam/GroundTruth/W.csv');
Z= csvread('F:/thesis3/selam/GroundTruth/K.csv');
SVMModel = fitcsvm(X,P,'Standardize',true,'KernelFunction','RBF',...
 'KernelScale','auto');
% test data
data2=[];
for i=1:2100
c=imread(strcat(['F:/thesis3/selam/Testingset/' num2str(i)],'.jpg'));
d=rgb2gray(c);
K=imresize(double(d),[ 512 512]);
features2= extractLBPFeatures(K);
data2=[data2;features2];
end
xtest=data2;
figure
Label = predict(SVMModel,xtest);
hold on;
plot(X(:,1),X(:,2),'ro','MarkerSize',12);
hold off
```

A.2 Implementation Code for GLCM using SVM

```
clear all
close all
clc;
data=[];
for i=1:4900
a=imread(strcat([' F:/thesis3/selam/Trainingset/' num2str(i)],'.jpg'));
b=rgb2gray(a);
glcm = graycomatrix(b,'Offset',[2 0],'NumLevels',16,'symmetric',true);
stats = graycoprops(glcm);
feat=[stats.Contrast stats.Correlation stats.Energy stats.Homogeneity];
data=[data;feat];
end
X=data;
```

```
P=csvread(' F:/thesis3/selam/GroundTruth/W.csv');
Z= csvread(' F:/thesis3/selam/GroundTruth/K.csv');
% SVMModel = fitclinear(X,P);
 SVMModel = fitcsvm(X,P,'Standardize',true,'KernelFunction','RBF',...
   'KernelScale','auto');
% test data
data2=[];
for i=1:2100
c=imread(strcat([' F:/thesis3/selam/Testingset/' num2str(i)],'.jpg'));
d=rgb2gray(c);
glcm = graycomatrix(d,'Offset',[2 0],'NumLevels',16,'symmetric',true);
stats = graycoprops(glcm);

feat2=[stats.Contrast stats.Correlation stats.Energy stats.Homogeneity];
data2=[data2;feat2];
end
xtest=data2;
Label = predict(SVMModel,xtest);
hold on;
plot(X(:,1),X(:,2),'ro','MarkerSize',12);
hold off
```

A3. Training

```
clc
clear
close all

TrainingDataPath = uigetdir('','Load Training Dataset');
Trainingimagefiles = dir([TrainingDataPath,'/*','.jpg']);

GroundTruthPath = uigetdir('','Load CSV File');
GroundTruthName = dir([GroundTruthPath,'/*','.csv']);

featurefromGLCMTraining =
featuresfrom('GLCM',TrainingDataPath,Trainingimagefiles);
featurefromLBPTraining =
featuresfrom('LBP',TrainingDataPath,Trainingimagefiles);

P=csvread([GroundTruthPath,'/' GroundTruthName.name]);

XTraining=[featurefromGLCMTraining featurefromLBPTraining];
Data = [XTraining P];
Mdl = fitclinear(XTraining,P);
saveCompactModel(Mdl,'code/SelamModel');
```

A4. Testing and Segmentation of the Exudates

```
clc
clear
close all

TestDataPath = uigetdir('','Load Test Dataset');
Testimagefiles = dir([TestDataPath,'/*','.jpg']);
Labeldatapath = uigetdir('','Load CSV File');
LabeldataName = dir([Labeldatapath,'/*','.csv']);
W=csvread([Labeldatapath,'/' LabeldataName.name]);

featurefromGLCMTest = featuresfrom('GLCM',TestDataPath,Testimagefiles);
featurefromLBPTest = featuresfrom('LBP',TestDataPath,Testimagefiles);

XTest=[featurefromGLCMTest featurefromLBPTest];
save('code/TestFeatures',XTest)

load SelamModel
save 'code/TestFeatures.mat' XTest W
[ind truep]=find(Label==1)
Detected =[];
for i = 1:length(ind)
    EXI=imread(['../testingset/' num2str(lind(i))],'jpg');
    Detected(i,:,:)=EXI;

EXI=imresize(I,[512 512]);
cd ..
figure,imshow(I);title('INPUT SOURCE IMAGE');
%%% step2 extracting the green channel component
R=I(:,:,1);
G=I(:,:,2);
B=I(:,:,3);
% F=histeq(G);
figure,imshow(G);title('GREEN CHANNEL COMPONENT');
%---apply  eqn (1) morphological closing operation for removing blobs
se=strel('disk',5);
C=imbothat(G,se);
figure,imshow(C,[]);title('FUNDUS REGION AFTER APPLYING MORPHOLOGICAL BOTTOM
HAT');
%-----------------------------------------------------
se=strel('disk',8);
H=imtophat(G,se);
figure,imshow(H,[]);title('FUNDUS REGION AFTER APPLYING MORPHOLOGICAL TOP
HAT');
tmp=im2bw(H-C,.18);
figure,imshow(tmp,[]);title('The detected exudates');
hold on;
u=contour(tmp,'b');
% G=imread()
% H=imread('untitled.png');
% figure;imshow(H);
a=tmp;
end

save Detected.mat Detected
```